THESIS

ADVANCED CAPACITY AND DISPATCH CO-DESIGN FOR THE TECHNO-ECONOMIC OPTIMIZATION OF INTEGRATED ENERGY SYSTEMS

Submitted by

Ziraddin Gulumjanli

Department of Systems Engineering

In partial fulfillment of the requirements

For the Degree of Master of Science

Colorado State University

Fort Collins, Colorado

Summer 2025

Master's Committee:

Advisor: Daniel R. Herber

Timothy C. Coburn
Vincent P. Paglioni
Jia Gaofeng

ABSTRACT

ADVANCED CAPACITY AND DISPATCH CO-DESIGN FOR THE TECHNO-ECONOMIC OPTIMIZATION OF INTEGRATED ENERGY SYSTEMS

This thesis explores the techno-economic performance of integrated energy systems by means of a linear optimization framework performed using direct transcription inside the DTQP environment. Over operational and financial time horizons, the model co-optimizes generating and storing technologies to maximize net present value (NPV) under different techno-economic assumptions. The basic dynamics of the subsystems are specified, with a special focus on balancing important physical and financial domains to enable effective decision-making within the framework of capacity and dispatch optimization.

Three sample case studies — natural gas with thermal storage, wind power with battery systems, and nuclear energy with hydrogen storage — are thoroughly analyzed in order to extend the basic concept, including sensitivity analysis. To assess their impact on ideal investment and deployment policies, key input parameters such as carbon tax levels, power and fuel prices, and capital and operating expenses are methodically changed. Results show that some factors, such as generator capital expenditures, especially electricity prices and energy prices, have an unusual influence on economic results, while others have little effect at all. These results are presented using scenario-specific outputs, comparison graphs, and trajectory-based insights, providing useful guidance on model robustness and decision-critical assumptions.

ACKNOWLEDGEMENTS

This thesis marks the culmination of an intense and rewarding chapter in my academic journey, and I would like to express my deepest gratitude to those who helped make it possible.

First and foremost, I am profoundly thankful to my advisor, Dr. Daniel R. Herber, for taking a chance on me and welcoming me into his lab. As the saying goes, after the storm, you are not the same person anymore — and that couldn't be more true of my time under his mentorship. I've grown not only through his deep technical knowledge and insightful guidance but also by observing his professionalism, patience, and the respect he consistently showed me. His influence has shaped me both as a researcher and as a person, and I am sincerely grateful for all the ways he's helped me evolve.

To my family — thank you for being my foundation. To my dad, for instilling in me resilience, discipline, and the strength to keep moving forward. To my mom, for her unwavering love, encouragement, and belief in me, especially during the uncertain moments. And to my sisters, thank you for always cheering me on and reminding me of my worth. Your belief in me means more than words can express.

I also want to extend my appreciation to the faculty who supported me along the way: Dr. Vinnie Paglioni, Dr. Steven Simske, Dr. Tim Coburn, and Dr. Erika Miller. Your thoughtful feedback, encouragement, and perspectives have made a lasting impact on the direction and depth of my work.

Two key projects during this period were deeply enriched by the mentorship of Joe Huyett and Dr. Saeed Azad. Working closely with them was an invaluable experience. Their technical expertise, practical problem-solving approaches, and willingness to guide and teach had a profound effect on how I think and operate. I learned so much from these collaborations, and I am grateful for the opportunities to grow under their leadership.

To everyone mentioned — and those who walked beside me quietly but faithfully — Thank You!

DEDICATION

To my family.

TABLE OF CONTENTS

LIST OF TABLES

LIST OF FIGURES

Chapter 1

Introduction

1.1 Integrated Energy Systems: Motivation and Concepts

Integrated energy systems (IESs) represent a paradigm shift in the conceptualization, operation, and assessment of modern energy systems. Historically, conventional energy systems for electricity, natural gas, heating and cooling, and hydrogen were developed in isolation with little interconnection. The combined efforts of urbanization, digitalization, climate regulation, and enhancements in system design have catalyzed a new generation of interconnected, multi-vector systems. To achieve enhanced flexibility, efficiency, and resilience across scales from the building to the national level [1], these systems integrate several energy carriers and infrastructures using both physical and virtual coupling technologies.

Power-to-gas (P2G) technologies and integrated heat and power units, which simultaneously provide thermal and electrical outputs, facilitate the use of excess or underutilized energy across several vectors. The fundamental principle of IES is to use synergies to enhance the equilibrium between supply and demand, reduce environmental impact, and bolster the overall resilience of energy service provision. In addition to technical systems, the connection encompasses the digital, financial, regulatory, and economic dimensions that affect energy system planning and operation [1].

From a systemic standpoint, IES has become clear as a necessary route to reach targets for the worldwide energy transition. The energy trilemma, which captures the simultaneous demand for decarbonization, supply security, and social acceptability, is a main force behind this integration. Thus, the move toward integrated systems is a reaction to complicated, linked policy and society goals as much as a technical reconfiguration. Often referred to as the total energy system approach, IES promotes novel interactions between energy production, distribution, and consumption across power, gas, heat, and transportation domains [2].

This whole-system view calls for fresh approaches to assessing energy efficiency. Integration brings about emergent behaviors and reciprocal interdependencies, requiring multidimensional evaluation systems that can handle technical, environmental, economic, and social effects simultaneously. Because they cannot adequately represent the extent and complexity brought forth by integration, existing assessment systems are typically insufficient. Thus, thorough evaluation approaches are required that can accommodate future uncertainties and balance trade-offs across several objectives and system levels [2].

Integrated energy systems seek to provide flexible, efficient, and sustainable energy services by leveraging the convergence of energy vectors, infrastructures, and markets, representing a conceptual and practical departure from previous models. In addition to a technological challenge, the development and deployment of such systems is strategically essential to align with long-term global energy and climate objectives [1, 2].

The historical development of energy systems models has paralleled the growing complexity of energy planning and policy, shifting from resource adequacy and cost-effectiveness to broader, long-term sustainability goals. Energy system models from the late 20th century mostly emphasized linear programming methodologies to facilitate fossil fuel-centric policy. More sophisticated modeling techniques are necessary to address the specific interdependencies of IES, since the twenty-first century presents climate challenges, renewable integration, and decentralization [3].

IES profoundly questions the hitherto compartmentalized character of national and regional energy systems. Integrated systems now need models that can account for interactions between supply and demand across vectors like energy, heat, hydrogen, and transportation, and resolve spatial and temporal variability. Especially when trying to evaluate the viability of high-renewable or hybrid systems depending on intermittent resources, conventional models fail to capture such characteristics. Emerging modeling techniques therefore seek to increase accuracy in real-time distribution, account for dynamic demand patterns, and include social elements and uncertainty in system-level assessments [3].

The shift toward hybrid systems, including nuclear-renewable systems, highlights even more the change in energy infrastructure paradigms. These systems are designed to take advantage of the complementary qualities of variable and dispatchable resources. For example, although wind power adds unpredictability and calls for balancing systems, nuclear generation offers a steady baseload. By allowing energy to be stored during times of surplus and recovered during shortages, thereby boosting both operational flexibility and economic performance, hydrogen storage is increasingly seen as a practical method to handle such fluctuation [4].

A clear example of integrated system architecture is a hybrid nuclear-wind system including hydrogen storage. This arrangement successfully decouples generation from demand by allowing both power generation and long-duration storage, unlike typical single-vector systems. This not only improves dependability but also helps decarbonization by allowing large proportions of renewables without sacrificing system economy. Particularly when based on modular and scalable nuclear technology, studies have demonstrated that such integration can boost the internal rate of return and raise grid responsiveness [4].

These illustrations together show the driving force behind integrated energy systems: the necessity to create flexible, multi-vector infrastructures capable of tackling challenging societal goals such as decarbonization, energy security, and affordability. IES presents a good basis for resilient and sustainable energy futures by using a systematic viewpoint, including technical, financial, and environmental layers [3, 4].

1.2 Coupling Mechanisms and Technologies in IES

In IES, an efficient capacity and deployment co-design depends on a thorough knowledge of the fundamental coupling technologies and physical mechanisms. This section reviews important coupling interfaces, system models, and operational dynamics, including P2G, CCS, and hydrogen-based systems, and highlighting their roles in improving flexibility, economic performance, and control inside integrated energy frameworks.

Combining Hydrogen Fuel Cells (HFCs), Carbon Capture and Storage (CCS), and P2G in local energy systems presents a complex approach to handle carbon reduction and renewable energy absorption. Two new modeling models [5] — PCH_SGWH (Power-to-Gas + CCS + HFC with Setting Gas With Heat) and PCH_SEWC (P2G + CCS + HFC with Setting Energy With Carbon) — allow complete coupling of electricity, gas, heat, and carbon flows within unified operational contexts. Constructed on coordinated plans, these models use HFCs for hydrogen-based cogeneration, CCS for CO_2 needed for methanation, and P2G for hydrogen-based conversion of excess power. Their main breakthrough is in recording energy-flow interactions and using control techniques to balance system costs, operational flexibility, and emissions [5].

P2G uses this design to turn extra renewable electricity into hydrogen, either methanated using collected CO_2 or straight utilized in HFCs to co-generate heat and electricity. Methanation allows excess hydrogen to be converted into synthetic methane using captured CO_2, enabling easier storage and compatibility with existing natural gas infrastructure. SGWH stresses cogeneration, guiding excess hydrogen to methanation, whereas SEWC promotes more general system-wide optimization by hydrogen and carbon interaction, controlling outputs. With up to 44.7% cost savings and 64.4% emissions reductions, simulation findings demonstrate SEWC provides exceptional wind integration and emissions reduction [5]. One important analytical realization is the hydrogen-carbon balance equation, fundamental to system operation. Here, carbon serves as a co-reactant to provide the strategic flexibility required to satisfy carbon objectives and accept fluctuating renewables; hydrogen serves as the internal energy vector.

Combining a stepped carbon pricing mechanism with a techno-economic dispatch model lets one evaluate system cost sensitivity to carbon policy. PCH_SEWC shows better economic viability under certain conditions [5]. These linked systems build a basis for low-carbon, high-flexibility infrastructures with great significance to regional energy and climate plans by linking electricity, gas, and heat networks, including carbon reuse. The indicator is proposed to measure coupling dynamics: directionality of energy conversion, separating capacity from real-time coupling. Case studies

and simulations show how different degrees of coupling affect system efficiency and operational constraints [6].

Harmonic instability due to frequency coupling and wideband control effects is first presented as a new challenge in converter-dominated systems. It presents as waveform distortion and grows worse with low Short-Circuit Ratio (SCR). High-order system integration is made possible with frameworks such as the Component Connection Method (CCM) by modeling techniques like state-space averaging, dq transformations, Harmonic State-Space (HSS), and Harmonic Transfer Functions (HTF) [7]. From an interdisciplinary perspective, multi-vector energy networks (MVELs) stress institutional layer and energy type integration. Three classes of coupling include local (downscale), system-wide (upscale), and cross-vector integration. Key physical interfaces include P2G and Combined Heat and Power (CHP). Interdependencies require coordinated controls, digital infrastructure, and regulatory harmonization [8].

To underline the need for coupling mechanisms in reaching low-carbon system design, a whole-systems modeling lens is important to grasp how both real-time and structural couplings affect dispatch methods and investment results [8]. Proposed for integrated energy planning is OMNI-ES, a bottom-up linear programming tool. It integrates CO_2 tracking and net-zero limitations and co-optimizes electricity, hydrogen, methane, and liquid fuel infrastructures across sectors and geographical nodes. Simulations demonstrate the ways in which hydrogen storage, carbon capture, renewables, and network enhancements help to reach climate objectives by capturing temporal and geographical fluctuations [9].

Emphasized as flexibility enablers are Power-to-X (P2X) technologies included in hybrid renewable energy systems (HRES). P2X promotes multi-sectoral energy flow by transforming excess power into chemical, thermal, or gaseous carriers. In many different fields, hydrogen is essential in connecting sporadic supply with demand. The gaps are observed in short-term dynamics and control in current HRES modeling, such as limited studies on day-ahead and real-time scheduling of P2X-integrated systems [10]. Advanced optimization and AI-based predictions are advised if

one is to fully maximize P2X potential. Hydrogen turns out to be the main primary vector for operational synergy across subsystems.

Some IES architectures rely on thermal energy storage (TES) to support the variable nature of renewable energy. It basically separates supply from demand by storing surplus heat generated at low-power rates or high renewable production and releasing it when peak energy demand arises. Sensible heat storage stores energy by increasing the temperature of materials such as water or stone. Latent heat storage relies on phase change processes, typically involving melting and solidification, to store energy. Sorption-based storage stores energy through reversible adsorption or absorption between working pairs. Among the several applications for every method — which have corresponding advantages — are residential heating, industrial thermal operations, building HVAC (heating, ventilation, and air conditioning) systems, and thermal power cycles. Combining TES into IES tightens the coupling across the electricity, heating, and transportation sectors as well as decreases renewable curtailment and boosts system flexibility [11].

Integration of TES into natural gas combined cycle (NGCC) plants with post-combustion carbon capture (PCC) presents one rather fascinating use for TES in flexible low-carbon power systems. Under this system, hot TES balances the parasitic thermal load connected with solvent regeneration for carbon capture, while cold TES cools the gas turbine inlet air to increase power production. Made to charge independently from plant operation, these TES subsystems maximize low-cost electricity during times of high renewable energy supply. Under thermodynamic and financial simulations, the integration of TES improves net present value (NPV), enhances dispatch flexibility, and strengthens the operational feasibility of NGCC + PCC systems, with the combined use of hot and cold TES delivering consistent financial benefits and the most favorable outcomes in every case [12].

Lastly, Integrated Demand Response (IDR) is introduced to exploit cross-vector flexibility by enabling energy carrier substitution — e.g., using gas or heat instead of electricity during peak load. Smart energy hubs and sectoral complementarity improve demand-side response, supporting system reliability and adaptability [13]. These coupling technologies and modeling frameworks

form the physical and operational backbone upon which advanced dispatch and planning strategies must be developed — linking real-world infrastructure to the optimization objectives explored in this thesis.

1.3 Modeling and Optimization Techniques for IES

Integrated control and decision-support systems capable of managing multi-vector interactions in real-time are desperately needed as IESs become more complex. The use of sophisticated optimization and machine learning (ML) techniques to enable coordinated planning and operation presents a potential path in this domain. These systems aim to co-optimize the management of energy carriers, including gas, heating, and electricity, under a single analytical framework. Furthermore, although ML allows exact forecasting and adaptive management in response to changing inputs such as renewable generation and consumer demand, optimization methods are crucial in the control of the practical details of cross-vector energy flow [14].

Recent studies provide a methodical classification of IES modeling techniques covering hybrid designs that combine data-driven prediction tools and independent optimization models. Principal applications of ML include demand pattern prediction, renewable energy output projection, and system performance anomaly identification. Combining ML insights into optimization processes enhances day-ahead planning, system adaptability, and operational decision-making under uncertain situations [14].

Although the application of optimization and ML methods to IES has advanced, completely integrated frameworks that run successfully in real-time situations still lag far behind. Particularly to support carbon-neutral energy goals via enhanced responsiveness and coordination across system levels, current research refers to the requirement of coherent architectures that mix predictive intelligence with optimization skills [14].

Advanced modeling approaches have evolved for regional integrated energy systems (RIES) in response to the increasing complexity and environmental sensitivity of energy infrastructures. One such strategy combines natural gas, thermal, and electrical networks on a single platform.

First, defining the structural and functional interdependencies among the subsystems, this framework then connects them using an energy hub model adept at organizing energy conversion and distribution decisions over vectors [7].

The key novelty of this approach is the integration into the optimization model of various carbon emissions trading schemes. This assures that environmental objectives — more notably, emissions reduction — are deeply rooted in economic cost control. For instance, carbon credits, such as the U.S. Section 45Q tax credit in [15], are precisely shown inside the techno-economic framework. Using the credit, which provides $\$85$ per metric ton of CO_2 sequestered over a 12-year period, the optimum deployment strategy of combined-cycle gas turbine facilities with carbon capture is shaped. The optimization model combines this policy incentive using a two-period NPV analysis, accounting for both the credit-eligible years and the subsequent non-credit years, so as to capture the changing economic situation during the lifetime of the plant. This approach ensures that incentives for emission reduction are not only included during the design stage but also directly influence operational decisions performed right now inside the energy hub architecture.

Conversely, the optimization model in [7] solved with the Fruit Fly Optimization Algorithm lets the energy hub act as a centralized coordinator distributing energy flows in real time, considering energy balance, equipment constraints, and external network restrictions. Three operating scenarios — following electricity demand, following heat load, and optimal scheduling — are used in testing the system.

In the larger framework of debates on IES, managing the uncertainty caused by changing demand and variable renewable energy generation is a key difficulty. A strong optimization framework has been proposed to address this challenge for the multi-objective planning of linked gas, heat, and power systems. This method develops a model that aims to concurrently minimize fuel costs, lower wind energy curtailment, and smooth out peak-valley disparities in power demand via a combination of strong optimization approaches that rely on particle swarm optimization (PSO) [16].

With an eye toward wind specifically, the suggested model views the IES as a whole, including natural gas pipelines, district heating systems, electric grids, and renewable sources [16]. Energy conversion ratios results show that well-coordinated planning across several linked subsystems may efficiently smooth out load variations and maximize energy conversion efficiency across several energy sources. The paper [16] also improves multi-energy system planning by adding a new goal — minimizing electrical load variance — to increase operational resilience under uncertainty. Using PSO and accounting for complicated conversions like P2H (power-to-heat) and H2P (heat-to-power), the proposed model achieves efficient energy allocation with optimal shares from outsourced electricity (31.29%), P2H (16.49%, power-to-heat), and G2H (13.56%, gas to heat).

A primary challenge to dispatch optimization in multi-energy systems (MES) is the seasonal fluctuation in energy demand and renewable resource availability, especially in systems that incorporate solar energy and combined cooling, heating, and power (CCHP) technologies. In this concept, Following Operation Cost (FOC) is suggested and assessed against more standard methods such as Following Electric Load (FEL) and Following Thermal Load (FTL) in order to handle this. Three criteria, such as operational cost (OC), carbon dioxide emissions, and primary energy consumption ratio, form the basis for the comparative assessment. Findings examined over several seasons help to reflect the dynamic performance of every method. Subsequently, a hybrid system is developed to produce better results in terms of cost-efficiency, emissions reduction, and energy usage of customization in dispersion modes to seasonal circumstances — employing FEL in winter and FOC during other months. These results underline the need for season-aware dispersion planning in the development of operational sustainability [17].

The many energy vectors and dynamic operating circumstances involved in multi-energy microgrids (MEMGs) have made the control and coordination of them more difficult. This is addressed by a hybrid control system combining fuzzy logic (FL) with model predictive control (MPC), therefore enhancing real-time energy management across the domains of power, heating, cooling, and hydrogen.

Unlike traditional static optimization methods, this intelligent control system enables adaptive and predictive operation, resulting in modest yet meaningful improvements: a 9.56% operating cost savings, a 2.8% CO_2 emissions reduction, and less reliance on gas and electric boilers [18]. Furthermore, the method raises the state of charge of storage facilities, therefore strengthening the MEMG's resilience and self-sufficiency. Reference [18] demonstrates how dynamically multifaceted multi-vector control systems can enhance efficiency and autonomy in distributed smart energy networks.

Expanding the operational scope of IES, a coordinated dispatch strategy explicitly involving district heating networks (DHNs) into the wider MES architecture is given [19]. This approach offers a two-layer DHN model comprising temperature correction equations and dispatch constraints to more clearly characterize the heat-power coupling across numerous CHP units than earlier models that either simplify or eliminate thermal transmission dynamics. An iterative optimization method decouples thermal and electrical fluxes, therefore allowing more responsive and efficient system coordination. Case studies in [19] based on an operational MES in Changchun, China, show that this method improves dispatch performance under varying wind generation and different heating demand. Consequently, the results show the strategic importance of DHNs in regulating CHP-centric MES settings and provide a scalable modeling approach for main thermal infrastructure development.

In the field of multi-energy systems, buildings act as dynamic energy nodes capable of offering both fast and delayed flexibility through assets including HVAC systems, lighting, electric vehicles (EVs), and battery storage. Developed to coordinate these resources inside hybrid building energy systems, a model-based predictive dispersion technique [20] helps to enable simultaneous participation in day-ahead energy markets, peak shaving programs, and ancillary service supply. Combining predictive optimization with a genetic algorithm lets the system distribute flexibility depending on user comfort limits and resource behavior. Results of simulations reveal a 26.1% decrease in power expenses, attained without sacrificing indoor environmental quality or battery

state-of-charge. By means of coordinated multi-service involvement, this framework positions buildings as active market players, therefore releasing operational and financial value.

Although the energy hub model has proven useful in the simulation of energy vector interactions, its simplified operational assumptions often fail to capture the full complexity of real-world system behavior. In response, the traditional energy hub framework via the incorporation of practical operational constraints that include part-load efficiency curves, equipment minimum runtimes, and storage degradation, is developed. These refinements allow for more accurate representation of system dynamics for devices such as heat pumps and thermal storage units, and remain compatible with mixed-integer linear programming (MILP) [21].

1.4 Techno-Economic Assessment and Control Co-Design for IES

Many aspects of the energy industry, including energy supply networks, transportation, storage, and consumption, have been profoundly affected by the always-shifting and rising energy demand coming from different technical breakthroughs, such as renewable energy and vehicle electrification. This rise in demand for power corresponds with environmental legislation imposing stricter carbon emissions criteria. Moreover, more consistent and flexible output will determine the stability of the electrical grid and the profitability of energy producers. Integration of several generating and storing systems offers a good way to adjust to such regulations and satisfy the rising energy consumption of our society [1]. This integration is positioned to transform the energy market economy and presents an integrated strategy towards energy systems [2].

Closely connected to IES [1] and hybrid energy systems (HES) [4], the integration of various generation and storage systems provides more flexibility and resilience of the energy supply/demand [22]. For certain utility firms, it also encourages fresh business models to better fit political, socioeconomic, scientific, technical, and financial changes. Utility companies are business entities; therefore, their long-term viability depends on consistent revenue generation (financial sustainability). Higher penetration of renewable energy sources, fluctuating fossil fuel prices,

stricter environmental rules, etc., however, might reduce the economic competitiveness of some technologies in combination.

For instance, the most costly per-unit electricity — often generated by nuclear power — is preferred last when other sources are not accessible owing to complexity, capital intensiveness, building time, etc. With little intermittency, the retirement of NPPs, which account for about a fifth of the total electricity output and half of the non-fossil fuel-based electricity generated in the United States, points to a shifting energy scene whereby NPPs need flexibility in base load to remain competitive [23].

By structuring such technologies as a component of integrated energy systems, running concurrently with other generators, functions like CCS, and energy storage units, one might perhaps boost their economic competitiveness. An NPP may, for instance, store energy during times of excess supply to maximize the selling price of energy. The stored energy can subsequently be sold straight as electricity or in another energy/complementary form, including thermal energy or hydrogen, depending on the storage method. While hydrogen may either be sold for use in fuel cells or the steel production sector, the thermal energy can be sold straight [24] to chemical plants for use in industrial operations.

The flexibility gained by including these generators in the framework of integrated energy systems must be adequate to overcome the capital and operational cost of the technology during its lifespan, therefore being economically viable. Often, at the center of examining how the integration of additional units (such as generator and storage) and functions (such as CCS, district heating/cooling, etc.) could influence the economics of the whole system is a techno-economic evaluation, expressed here as an NPV target. It is also fundamental in any retrofit design project inside a structured energy system.

Capacity and dispatch optimization help to maximize NPV by means of storage capacities (i.e., plant variables), sought power, charge, and discharge decisions (i.e., control variables). Control co-design (CCD) [25] is the result of this combination and design choice consideration. Integrated energy systems for an NGCC with TES and CCS [26], light water reactor (LWR) with

various TES technologies [23], and a nuclear power plant with hydrogen production [27] have been investigated in the framework of this class of problems.

When applied with high-fidelity, non-linear technical models, the resultant dynamic optimization problem is typically computationally costly. For example, [28] considered a 24-hour horizon and solved the problem 365 times, therefore lowering the computational cost compared to solving the problem for a complete year. Effective early-stage decision-making calls for ideally minimal assumptions and changes outside the basic techno-economic ones required for evaluation. To evaluate different system configurations and scenarios for integrated generator and storage energy systems, an effective and flexible computational framework that can capture subsystems' basic dynamics, restrictions, and NPV economic analysis is very much needed.

The fact that feasibility assessments of several system configurations/architectures are usually needed before choosing the most advantageous solution motivates this computational framework even more. By considering the fundamental dynamics of subsystems, one may evaluate several system designs with flexibility without devoting a prohibitive amount of resources to the research, building, and optimization of high-fidelity models. The balance of authenticity maintained in the proposed framework helps to evaluate general system performance without the necessity of determining particular subsystems and components, since particular system components, characteristics, and performance criteria are often unknown in early-stage design and will be decided in later steps. Ultimately, a flexible framework should enable engineers with technical expertise in the area, as well as those with less technical backgrounds, such as stakeholders and investors, who are often among the main decision-makers in the sector, to negotiate the decision-making process.

1.5 Sensitivity and Uncertainty Analysis in Integrated Energy Systems

The growing complexity of IESs makes knowledge of their behavior under uncertainty essential for guaranteeing strong design and optimal operation. Sensitivity analysis is a recognized method

employed to examine the effects of variations in design parameters, external factors, and policy choices on system performance and resilience.

Using sensitivity models to assess the cost of carbon emission reduction (CER) techniques at both local and global levels, [29] presented a bi-objective optimization framework to concurrently reduce operational costs and carbon emissions. The study produced an equally distributed Pareto frontier to enable decision-making without depending on subjective assumptions and highlighted how system flexibility — defined by thermal inertia and battery capacity — impacts operational results [29].

Within the framework of building-integrated energy systems, a main design difficulty is unpredictability resulting from user behavior, environmental circumstances, and energy market volatility. Mixed-integer linear programming was used to assess, using a sensitivity-based approach, how these uncertainties affect the ideal layout of building systems [30]. The results of the sensitivity analysis indicate that equipment sizes can vary by up to 100% when robustness is considered, compared to systems designed using traditional deterministic methods. The authors of [30] underlined, therefore, that the necessity of strong techniques is system-specific and advised a practical first step of deterministic sensitivity analysis.

Sensitivity analysis has also been extended to linked electricity-heating systems, in which dynamic interactions between subsystems are bidirectional. The effect of distributed coupling units on general system behavior was investigated using a technique utilizing sensitivity factors obtained from a coupled Newton-Raphson power flow model [31]. Particularly in systems running in both power-led and heat-led modes, this method achieved calculation time savings of up to eightfold and enhanced accuracy over conventional electric-only sensitivity measurements.

These studies demonstrate how sensitivity and uncertainty analysis facilitate informed decision-making in the design and operation of IES, thereby enabling planners to predict the consequences of parameter variability, increase flexibility, and enhance system-wide resilience.

1.6 Thesis Overview

This work offers the creation and proof of an open-source framework in MATLAB for evaluating the *economic feasibility of generator and storage systems through CCD*, thus referred to as ECOGEN-CCD. Inspired by basic dynamics of subsystems, ECOGEN-CCD develops the capacity and dispatch dynamic optimization problem that can be effectively implemented and solved using the open-source MATLAB software DTQP [32, 33], which uses direct transcription with an automated optimization problem generation for linear-quadratic dynamic optimization problems. ECOGEN-CCD is an open-source tool that is made publicly available in [34].

1.6.1 Significance

This research looks at a critical decision support problem in the (integrated) energy systems domain that has to be solved quickly and repeatedly to help decision makers move toward energy systems that are more sustainable, robust, and cost-effective. The proposed optimization-based framework meets this challenge by combining the fundamental technical design and financial sustainability of IES with a CCD framework that directly maximizes NPV within the limits of practical operations. Furthermore, the basic IES architecture supports investigations into many different technologies and policy settings with flexibility for future expansion. In the system development lifecycle, this work focuses on making early-stage decisions with the necessary techno-economic rigor, as demonstrated by several IES case studies involving diverse generator and storage technologies. This framework differs from many previous models in that it is specifically designed to balance model fidelity/details and evaluation time, resulting in a valuable framework for both technical analysts and high-level stakeholders.

1.6.2 Remaining Content

The remainder of the thesis is organized in the following manner: Chapter 2 starts by describing some motivations for the proposed framework and then discusses optimization framework architecture, problem elements, techno-economic considerations, and problem formulation. Chapter 3

is focused on the demonstration of the proposed framework using three case studies with different generator and storage technologies, including an NGCC with TES and CCS, wind energy with battery energy storage, and an NPP with hydrogen generation and storage. In addition to presenting baseline optimization results, the chapter includes comprehensive sensitivity analyses for each scenario to assess the impact of key techno-economic parameters on system design, operation, and economic performance. Chapter 4 summarizes the key findings, discusses the limitations of the current framework, and outlines potential directions for future work, including model expansion, integration with uncertainty quantification, and real-time operational considerations.

Chapter 2

Methodology

2.1 Design Framework for Integrated Energy Systems

This section delineates the IES architecture, problem components, techno-economic factors, and the capacity and dispatch optimization problem.

Figure 2.1 describes the general architecture of an IES considered in this framework. A variety of generators (e.g., natural gas combined cycle (NGCC) power plant, wind farm, or nuclear power plant (NPP)) and storage units (e.g., thermal energy storage (TES), battery energy storage system (BESS), or hydrogen storage) define an Integrated Energy System. The system could also incorporate additional purposes (such as district heating and cooling, CCS, etc.), which differ in associated expenditures and energy demand.

The generator unit in this thesis is described by the subscript $\bullet_G$, and responsible to produce electricity from an energy vector (e.g., natural gas) by often converting it first to a primary energy domain (e.g., thermal energy), and ultimately converting it to electricity with efficiency of η_G:

$$\text{generator's primary energy domain} \xrightarrow{\eta_G} \text{electricity} \tag{2.1}$$

The intended IES configuration suggests that the generator may have access to three distinct kinds of storage systems, categorized through the subscript $\bullet_S$. Those storage systems are described based on their key energy domain. The first storage system uses the generator's primary domain, $\bullet_P$, to store energy. In an NGCC power plant, for instance, thermal energy dominates all other energy categories and is the primary energy domain. For this generator, thus, a TES unit serves as the primary storage mechanism. In this work, the secondary energy domain is always electrical, $\bullet_E$. Therefore, the second storage type directly stores energy as electricity (e.g., through a BESS). A third storage facility, on the other hand, $\bullet_T$, is included to enable the usage of electricity to develop a new product, commodity, service, or energy storage in a distinct medium, such as hydrogen. The

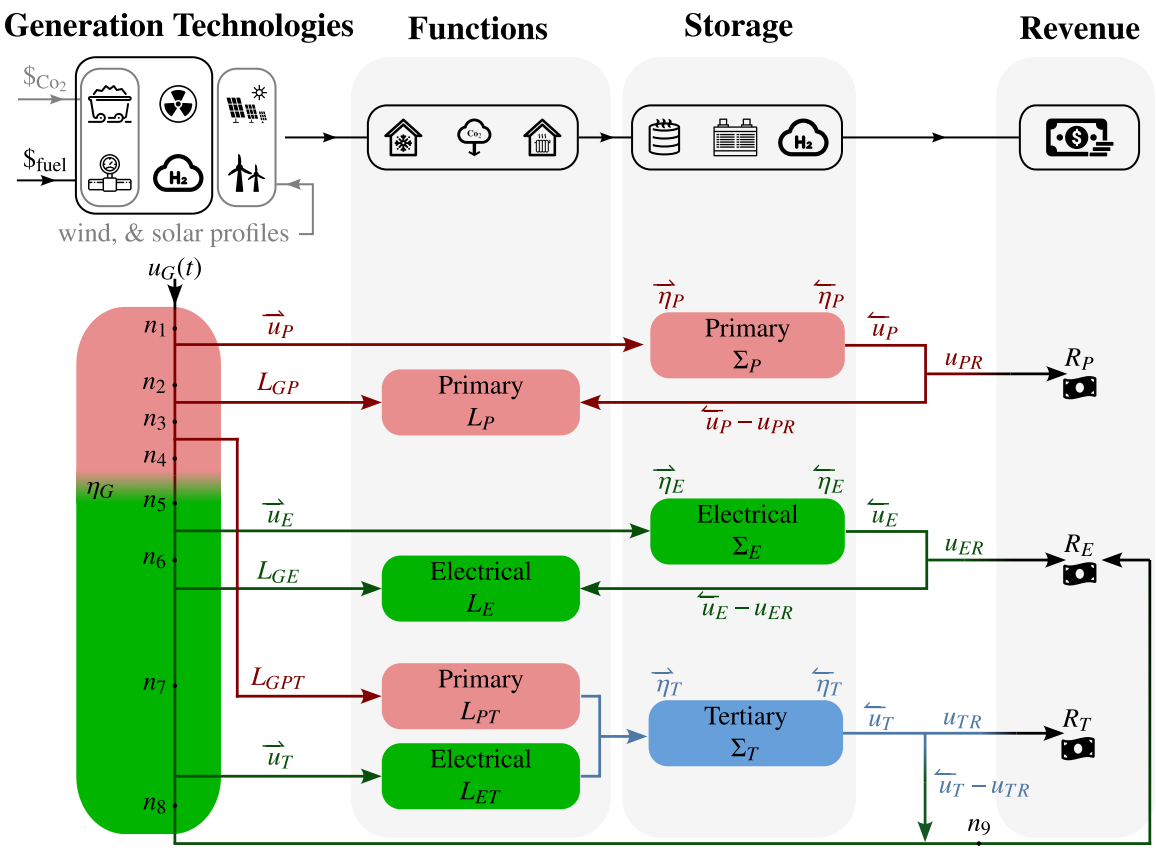

Figure 2.1: Illustration of ECOGEN-CCD integrated energy system (IES) architecture

storage system is characterized by charge $\overrightarrow{\bullet}$ and discharge $\overleftarrow{\bullet}$ signals, with attention to the orientation of the arrows. Energy drops over the transmission process might influence the charge signal. Consequently, its efficiency is represented as $\overrightarrow{\eta}_\bullet$. The storage's output efficiency is characterized as $\overleftarrow{\eta}_\bullet$:

$$\text{charging signal} \xrightarrow{\overrightarrow{\eta}_\bullet} \text{storage} \tag{2.2a}$$

$$\text{storage} \xrightarrow{\overleftarrow{\eta}_\bullet} \text{discharge signal} \tag{2.2b}$$

This reasonable classification of efficiencies helps us to consider future additional factors, including the distance between facilities, which might affect the efficiency of energy transmission. Denoted as $\bullet_R$, a supplemental revenue-oriented control signal finds the percentage of the discharge signal that is immediately turned into revenue via direct sales. For example, the quantity

of released hydrogen sold at current hydrogen pricing will be found from the revenue signal. The remaining product will be burned and sold as power.

Including several purposes might lead to additional load needs. For instance, running a CCS unit — assumed to be in operation anytime the generator is on — requires extra thermal and electrical demands in addition to auxiliary electrical loads. Shown as a particular proportion of the energy level of the power plant, these loads depend on the present power level of the generator. In a hydrogen plant (tertiary storage), a high-temperature steam electrolysis (HTSE) process also requires both thermal and electrical energy. These load needs, however, are active only once a choice is taken to produce hydrogen from the surplus power. These loads rely on the tertiary charging signal, expressed as a particular proportion of its present value.

The upper section of Figure 2.1 covers some details on the electric energy technologies, including fuel cost, carbon tax, and dispatchable versus non-dispatchable types of resources. The lower section illustrates a case for a collection of homogeneous generators (e.g., a wind farm) in the presence of multiple functions and storage types. The nodes in this figure, which are described by $n_1, \ldots, n_9$ are used to formulate some of the necessary constraints within the optimization problem and are mathematically described in Table 2.1.

2.2 Problem Variables

This section addresses specific issue factors derived from a thorough example, including a set of homogenous generators with possible access to all three storage types in between, both primary and electrical loads. The future phase of this effort will involve the integration of the capability to concurrently operate numerous non-homogeneous generators. In the future, it is anticipated that a more sophisticated integration of storage units inside the toolbox would allow for the simultaneous incorporation of several storage topologies (e.g., two battery storage units and one hydrogen storage unit) with ECOGEN-CCD.

Plant Variables: The capacity of each storage type is a size selection determined by the optimizer and signifies the variables for plant optimization $\boldsymbol{\Sigma}$:

$$\boldsymbol{\Sigma} = [\Sigma_P, \Sigma_E, \Sigma_T]^T \tag{2.3}$$

Note that the vector of plant optimization variables reduces in size if the study does not include all three storage types.

Control Variables: In total, four types of control variables are presented and divided into two parts: storage and generator variables. Every energy storage system involves three control variables, one for charging the storage ($\overrightarrow{u_\bullet}$), one for discharging the storage $\overleftarrow{u_\bullet}$, and one for determining the fraction of discharge $u_{\bullet R}$ that is directly used to generate revenue without any intermediate steps. In addition, the operator can request a specific power from the generator through a control command, described as $u_G(t)$. The vector of control variables can then be defined as:

$$\begin{aligned} \boldsymbol{u}(t) &= [u_G(t), \boldsymbol{u}_S(t)]^T \\ &= [u_G(t), \boldsymbol{u}_{SP}(t), \boldsymbol{u}_{SE}(t), \boldsymbol{u}_{ST}(t)]^T \end{aligned} \tag{2.4}$$

Here, every storage control vector $\boldsymbol{u}_{S\bullet}(t)$ consists of three variables:

$$\boldsymbol{u}_{S\bullet}(t) = [\ \overrightarrow{u_\bullet}(t),\ \overleftarrow{u_\bullet}(t), u_{\bullet R}(t)]^T \tag{2.5}$$

As in the prior situation, the size of the control vector depends on whether certain storage types are incorporated into the analysis.

State Variables and Associated Dynamics: One state variable pertains to the generator, which defines its power level with a specified ramp rate of τ:

$$\dot{x}_G(t) = \frac{1}{\tau}(-x_G(t) + u_G(t)) \tag{2.6}$$

Each storage system is characterized by a state variable that denotes the current accessible amount of stored energy inside that system.

For the most comprehensive scenario, where three different storage facilities are included, the storage dynamics are described by:

$$\dot{\boldsymbol{x}}_S(t) = \begin{bmatrix} \dot{x}_P(t) \\ \dot{x}_E(t) \\ \dot{x}_T(t) \end{bmatrix} = \overbrace{\begin{bmatrix} \overrightarrow{\eta}_P \, \overrightarrow{u}_P(t) \\ \overrightarrow{\eta}_E \, \overrightarrow{u}_E(t) \\ \alpha_{ET} \, \overrightarrow{\eta}_T \, \overrightarrow{u}_T(t) \end{bmatrix}}^{\text{Charge}} - \overbrace{\begin{bmatrix} \overleftarrow{u}_P(t) \\ \overleftarrow{u}_E(t) \\ \overleftarrow{u}_T(t) \end{bmatrix}}^{\text{Discharge}} \tag{2.7}$$

where α_{ET} denotes the conversion rate from electricity to the tertiary commodity. The problem dynamics are expressed by specifying storage states in vector format and augmenting them with the generator state.

$$\dot{\boldsymbol{x}}(t) = \boldsymbol{A}\boldsymbol{x}(t) + \boldsymbol{B}\boldsymbol{u}(t) \tag{2.8}$$

$$\begin{bmatrix} \dot{x}_G(t) \\ \dot{\boldsymbol{x}}_S(t) \end{bmatrix} = \begin{bmatrix} -1/\tau & \mathbf{0} \\ \mathbf{0} & \mathbf{0} \end{bmatrix} \begin{bmatrix} x_G(t) \\ \boldsymbol{x}_S(t) \end{bmatrix} + \begin{bmatrix} 1/\tau & \mathbf{0} \\ \mathbf{0} & \boldsymbol{b}_S \end{bmatrix} \begin{bmatrix} u_G(t) \\ \boldsymbol{u}_S(t) \end{bmatrix}$$

where $\boldsymbol{b}_S$ is the appropriately-sized matrix:

$$\boldsymbol{b}_S = \begin{bmatrix} \overrightarrow{\eta}_P & -1 & 0 & 0 & 0 & 0 & 0 & 0 & 0 \\ 0 & 0 & 0 & \overrightarrow{\eta}_E & -1 & 0 & 0 & 0 & 0 \\ 0 & 0 & 0 & 0 & 0 & 0 & \alpha_{ET} \, \overrightarrow{\eta}_T & -1 & 0 \end{bmatrix} \tag{2.9}$$

2.3 Additional Constraints and Objective Function

Constraints

This section presents all of the time-independent and time-dependent constraints in the dynamic optimization problem.

The storage capacities are non-negative. Therefore, the following constraint is imposed on plant variables: each storage-related decision variable must satisfy a minimum value threshold of zero to ensure physical feasibility.

$$\mathbf{0} \leq \mathbf{\Sigma} \tag{2.10}$$

The power required from the generator must be non-negative and must not surpass the generator's net nominal capacity. Similarly, the charge and discharge signals are non-negative and do not surpass the maximum energy transfer rates into and out of the storage system, respectively. The current input parameters for maximum and minimum energy transfer rates will be included in the array of potential plant optimization elements in the future, akin to [26]. The restrictions are concisely articulated in vector notation as:

$$\mathbf{0} \leq \boldsymbol{u}(t) \leq \boldsymbol{u}_{\max}(t) \tag{2.11}$$

The revenue-generating component of the control signal in Eq. (2.11) is non-negative and less than or equal to the discharge signal:

$$u_{PR}(t) \leq \overleftarrow{u}_P(t) \tag{2.12a}$$

$$u_{ER}(t) \leq \overleftarrow{u}_E(t) \tag{2.12b}$$

$$u_{TR}(t) \leq \overleftarrow{u}_T(t) \tag{2.12c}$$

The power output of the generator must be non-negative and not more than its nominal capacity. For systems like nuclear or natural gas combined cycle (NGCC), requesting a specific allowed power output from the generator is reasonable, given simplifying presumptions that include the absence of temperature dependency on operation or maintenance schedules. Solar and wind intermittent technologies rely on the availability of renewable resources. The intrinsic intermittency of the resource makes the electricity produced by such technologies non-dispatchable. Consequently, it is imperative to control the generator state $x_G(t)$ by an input signal denoting the degree

of resource availability. This results in the later restriction on the state of the generator:

$$\boldsymbol{x}_{G,\min}(t) \leq \boldsymbol{x}_G(t) \leq \boldsymbol{x}_{G,\max}(t) \tag{2.13}$$

where $\boldsymbol{x}_G(t)$ denotes the generator's state, and $\boldsymbol{x}_{G,\max}(t)$ is an upper bound that is established based on nominal capacity, or the availability of renewable resources. Further details that cover the construction of $\boldsymbol{x}_{G,\max}(t)$ for a wind farm are included in Section 3.2.

The stored energy amount has to be non-negative and less than the storage system's capacity:

$$\mathbf{0} \leq \boldsymbol{x}_S(t) \leq \boldsymbol{\Sigma} \tag{2.14}$$

which shows a fundamental link between some states and the plant characteristics. For all the state variables, the beginning states are prescribed. Furthermore, it is assumed that the storage system has the same stored energy level at t_0 as the last time t_f:

$$\boldsymbol{x}(t_0) = \boldsymbol{x}_0 \tag{2.15a}$$

$$\boldsymbol{x}_S(t_f) = \boldsymbol{x}_S(t_0) \tag{2.15b}$$

where the latter equation is optional as certain shorter, consecutive time spans do not require this assumption [26].

Apart from the upper limit set by the maximum energy transfer rate for charging the storage system in Eq. (2.11), it is essential to guarantee that the charging signal is smaller than or equal to the available power in the generator. This is explained with the aid of nodes arranged in Figure 2.1:

$$\overrightarrow{u}_P(t) \leq n_1(t) \tag{2.16a}$$

$$\overrightarrow{u}_E(t) \leq n_5(t) \tag{2.16b}$$

$$\overrightarrow{u}_T(t) \leq n_7(t) \tag{2.16c}$$

where Table 2.1 provides the mathematical equations connected with all the nodes $n_1, \ldots, n_9$.

Furthermore, the generator's load-satisfying signals L_{GP}, L_{GE}, and L_{PT} are non-negative. This condition ensures that electricity does not transfer from the storage system to the generator. These signals are likewise constrained by the generator's available power. These constraints are formulated as:

$$\mathbf{0} \leq L_{GP}(t) \leq n_2(t) \tag{2.17a}$$

$$\mathbf{0} \leq L_{GPT}(t) \leq n_3(t) \tag{2.17b}$$

$$\mathbf{0} \leq L_{GE}(t) \leq n_5(t) \tag{2.17c}$$

Objective Function

In this study, the objective function is the maximization of Net Present Value to evaluate the economic feasibility of a given technology, which is calculated as:

$$\text{maximize} \quad \text{NPV} = -C_{\text{cap}}(\boldsymbol{\Sigma}) + \int_{t_0}^{t_f} \frac{v_{\text{profit}}(\boldsymbol{u}, \boldsymbol{x}, \boldsymbol{\Sigma}, t)}{D(t)} dt \tag{2.18}$$

where C_{cap} are the capital expenses, $v_{\text{profit}}(t)$ is calculated as a function of expenses and revenues, and $D(t)$ is the discounting function (money is 'worth' more now than in the future). A more detailed explanation of techno-economic parameters is provided in the next chapter. An annualized discounting function is defined as follows:

$$D(t) = (1 + r)^{\text{year}(t)} \tag{2.19}$$

where r is the discount rate and year(t) is the integer number of years that have passed since t_0. These intermediate quantities are now discussed in detail.

Table 2.1: Node signal definitions with lexical interpretation from Figure 2.1

Lexical interpretation	**Mathematical description**
Initial available primary-type power	$n_1 : x_G$
Available primary-type power after charging primary storage units	$n_2 : x_G - \overrightarrow{u}_P$
Primary power available after fulfilling the primary load requirements	$n_3 : x_G - \overrightarrow{u}_P - L_{GP}$
Primary power available after meeting the primary load for tertiary operations	$n_4 : x_G - \overrightarrow{u}_P - L_{GP} - L_{GPT}$
Electrical power available after considering power conversion efficiency	$n_5 : \eta_G(x_G - \overrightarrow{u}_P - L_{GP} - L_{GPT})$
Electrical power available after charging the electrical storage	$n_6 : \eta_G(x_G - \overrightarrow{u}_P - L_{GP} - L_{GPT}) - \overrightarrow{u}_E$
Electrical power available after meeting the electrical load demand	$n_7 : \eta_G(x_G - \overrightarrow{u}_P - L_{GP} - L_{GPT}) - \overrightarrow{u}_E - L_{GE}$
Electrical power available after meeting the electrical load requirements for tertiary operations	$n_8 : \eta_G(x_G - \overrightarrow{u}_P - L_{GP} - L_{GPT}) - \overrightarrow{u}_E - L_{GE} - \overrightarrow{u}_T$
Electrical power available after burning the tertiary product	$n_9 : \eta_G(x_G - \overrightarrow{u}_P - L_{GP} - L_{GPT}) - \overrightarrow{u}_E - L_{GE} - \overrightarrow{u}_T + \alpha_c \overrightarrow{\eta}_T \overrightarrow{u}_T - \alpha_c \overrightarrow{\eta}_T u_{TR}$
The generator's primary energy output to satisfy the primary load demand	$L_{GP} = L_P x_G - \overrightarrow{\eta}_P \overrightarrow{u}_P + \overrightarrow{\eta}_P u_{PR}$
Primary power provided by the generator to fulfill the primary load demand for tertiary operations	$L_{GPT} = L_{PT} \overrightarrow{u}_T$
Electricity generated to fulfill the electrical load demand	$L_{GE} = L_E x_G - \overrightarrow{\eta}_E \overrightarrow{u}_E + \overrightarrow{\eta}_E u_{ER}$

2.4 Tehno-Economic Considerations

First, the sources of revenue and expenses in Eq. (2.18) are examined to develop the NPV objective function, where its negative value in the results shows profit while a positive value shows loss.

Expenses

All expenses included in the techno-economic study — capital expenditures, constant and variable operations and maintenance costs, fuel expenses, carbon tax prices — are listed in this section.

Capital Costs: In this thesis, it is assumes that the capital cost, C_{cap} ,consists of overnight capital costs defined as C_{occ}, and costs carried over the period of construction represented as C_{cp}:

$$C_{\text{cap}} = C_{\text{occ}} + C_{cp} \tag{2.20}$$

where C_{occ} supposes that all the building takes place instantaneously. This eliminates changes in the cost of products and financial expenses (including the loan, inflation, discount rate, etc.). This enables possible studies in the analysis [35] on the influence of building periods, inflation rates, etc. Expanded in great depth in [36, 37], C_{occ} comprises direct construction costs, indirect construction costs, contingencies, and the owner's cost.

C_{cp} covers all expenses, including financing, inflation, escalation, etc., accumulated throughout the construction time. This parameter is sensitive to the choice of financial factors, including discount rate, debt-equity ratio, interest rate, interest during construction (IDC), etc. In this study, this term is simplified similarly to the methodology presented in [38], to account for the costs over the period of construction through a simple model characterizing IDC:

$$C_{\text{cap}} = C_{\text{occ}}(1 + C_{\text{idc}}) \tag{2.21}$$

where C_{idc} is calculated as a function of the construction time T_{con}, and the discount rate r is estimated as:

$$C_{\text{idc}} = \frac{r}{2} T_{\text{con}} + \frac{r^2}{6} T_{\text{con}}^2 \tag{2.22}$$

Inclusion of more advanced financial parameters [26], such as loan, depreciation, etc., is a future work item for this framework. Entirely, ECOGEN-CCD's capital cost is expressed as:

$$C_{\text{cap}} = [C_{\text{occ}_G} + C_{\text{occ}_P}\Sigma_P + C_{\text{occ}_E}\Sigma_E + C_{\text{occ}_T}\Sigma_T](1 + C_{\text{idc}}) \tag{2.23}$$

Operation and Maintenance (O&M): Fixed and variable O&M costs define the primary components of O&M expenses. Expressed as C_{fom}, fixed O&M expenses comprise routine system maintenance, decommissioning, component replacement, etc. These expenses rely solely on the duration of the operation. For storage systems, these expenses vary with storage capacity (e.g., higher capacities necessitate more frequent and prolonged maintenance).

Fixed O&M costs C_{fom} are then calculated as:

$$C_{\text{fom}}(t) = C_{\text{fom}_G} + C_{\text{fom}_P}\Sigma_P + C_{\text{fom}_E}\Sigma_E + C_{\text{fom}_T}\Sigma_T \tag{2.24}$$

Variable O&M costs, expressed as C_{vom}, reflect the non-fuel portion of the costs that vary by the amount of energy generated or supplied (such as water usage, waste disposal fees, lubricants, cooling agents, treatment chemicals, and other consumable operating materials that are depleted or used in proportion to output). Therefore, these costs depend on the power level of the unit, expressed as:

$$C_{\text{vom}}(t) = C_{\text{vom}_G}\boldsymbol{x}_G(t) + C_{\text{vom}_P}(\ \overrightarrow{\eta_P}\ \overrightarrow{u_p}(t) + \overleftarrow{u_p}(t)\ ) \tag{2.25a}$$

$$+ C_{\text{vom}_E}(\ \overrightarrow{\eta_E}\ \overrightarrow{u_E}(t) + \overleftarrow{u_E}(t)\ ) \tag{2.25b}$$

$$+ C_{\text{vom}_T}(\ \alpha_{ET}\ \overrightarrow{\eta_T}\ \overrightarrow{u_T}(t) + \overleftarrow{u_T}(t)\ ) \tag{2.25c}$$

Fuel Costs: The fuel cycle cost, defined as $C_{\text{fuel}}(t)$, encompasses both front-end and back-end for nuclear components — such as supply, conversion, enrichment, fabrication, transportation, and waste disposal — whereas for fossil fuels, it typically includes only the front-end costs as received directly from the market.

On nuclear power plants, however, the back-end expenses defined as $E_{\text{fuel}}(t)$ also factor as a fraction of the front-end expenses:

$$E_{\text{fuel}}(t) = \rho_{\text{fuel}} C_{\text{fuel}}(t) x_G(t) + B_{\text{fuel}}(t) \tag{2.26}$$

where ρ_{fuel} is the conversion factor between the power output of the generator and fuel consumed, $C_{\text{fuel}}(t)$ is the instantaneous fuel price, and $B_{\text{fuel}}(t)$ is the back-end cost (again, mainly necessary for waste management and disposal in nuclear power plants).

Carbon Cost: To render the societal cost of carbon emissions apparent, carbon cost, denoted as CO_2, adopts a carbon tax rate to promote the creation of clean power. The cost of carbon is therefore calculated as:

$$E_{CO_2}(t) = C_{CO_2} \alpha_{CO_2} \rho_{\text{fuel}} x_G(t) \tag{2.27}$$

where C_{CO_2} is the carbon tax, and α_{CO_2} is the amount of CO_2 produced per unit of fuel.

Revenue

The operator can make money, either directly selling power to the grid without using storage or using storage to sell primary energy, electricity, or a tertiary product. Using their different prices, the total income is calculated for every energy industry. The optimum energy flow that maximizes the target function is dictated by price arbitrage among main, electrical, and tertiary sectors.

As an example, revenue earned by selling stored thermal energy to chemical plants (first term in Eq. (2.28)) is calculated as a function of thermal energy prices $C_P(t)$, discharge efficiency $\overleftarrow{\eta}_P$, and the revenue control signal $u_{PR}(t)$. The revenue control signal may turn on mostly at times

when thermal energy costs are quite high and electricity prices are low, allowing the system to optimize economic gains by using suitable market circumstances. This technique enables deliberate action of system components to convert and store energy in forms that provide more returns. For some commodities, including hydrogen, electricity may be used to create the commodity, which can then be stored and later sold back to the grid when market prices are favorable. This gives the system more adaptability and financial viability. Mathematically, one may characterize the resultant income from these activities as:

$$
\begin{aligned}
R &= R_P(t) + R_E(t) + R_T(t) \\
&= C_P(t)\,\overleftarrow{\eta}_P u_{PR}(t) + C_E(t)\eta_G x_G(t) - C_E(t)\eta_G\,\overrightarrow{u}_P(t) \\
&\quad - C_E(t)\eta_G L_P x_G(t) + C_E(t)\eta_G\,\overleftarrow{\eta}_P\,\overleftarrow{u}_P(t) \\
&\quad - C_E(t)\eta_G\,\overleftarrow{\eta}_P u_{PR}(t) - C_E\eta_G L_{PT}\,\overrightarrow{u}_T - C_E(t)\,\overrightarrow{u}_E(t) \\
&\quad - C_E(t)L_E x_G(t) + C_E(t)\,\overleftarrow{\eta}_E\,\overleftarrow{u}_E(t) - C_E(t)\,\overrightarrow{u}_T(t) \\
&\quad + \alpha_{\text{TE}} C_E(t)\,\overleftarrow{\eta}_T\,\overleftarrow{u}_T(t) - \alpha_{\text{TE}} C_E(t)\,\overleftarrow{\eta}_T u_{TR}(t) \\
&\quad + C_T(t)\,\overleftarrow{\eta}_T u_{TR}(t)
\end{aligned}
\tag{2.28}
$$

where:

- $C_P(t)$: price of the primary energy (e.g., natural gas, coal, or biomass)
- $C_E(t)$: electricity market price at time t
- $C_T(t)$: price of the tertiary commodity or product (e.g., hydrogen, heat, or other value-added outputs)

2.5 Optimization Problem Formulation

Upon identifying all problem elements, the economic feasibility of a potential IES may be assessed through the optimization of capacity and dispatch within a thorough problem formulation:

$$
\begin{aligned}
\text{changing:} \quad & \boldsymbol{u}(t), \boldsymbol{x}(t), \boldsymbol{\Sigma} && \text{(2.29a)} \\
\text{maximize:} \quad & \text{NPV}(t, \boldsymbol{u}, \boldsymbol{x}, \boldsymbol{\Sigma}, \boldsymbol{d}) && \text{(2.29b)} \\
\text{subject to:} \quad & \boldsymbol{g}(t, \boldsymbol{u}, \boldsymbol{x}, \boldsymbol{\Sigma}, \boldsymbol{d}) \leq \boldsymbol{0} && \text{(2.29c)} \\
& \dot{\boldsymbol{x}} - \boldsymbol{f}(t, \boldsymbol{u}, \boldsymbol{x}, \boldsymbol{\Sigma}, \boldsymbol{d}) = \boldsymbol{0} && \text{(2.29d)} \\
& \boldsymbol{x}(t_0) = \boldsymbol{x}_0 && \text{(2.29e)} \\
& \boldsymbol{x}(t_f) = \boldsymbol{x}(t_0) \text{ (optional)} && \text{(2.29f)} \\
\text{where:} \quad & \boldsymbol{u} = \boldsymbol{u}(t), \ \boldsymbol{x} = \boldsymbol{x}(t) && \text{(2.29g)} \\
& t \in [t_0, t_f], \ t_f = N t_p && \text{(2.29h)}
\end{aligned}
$$

with:

- $\boldsymbol{d}$ is the vector of problem parameters.
- $\boldsymbol{g}(\cdot)$ is the vector of inequality constraints, associated with Eqs. (2.10)–(2.17c).
- Equation (2.29d) refers to system dynamics described in Eqs. (2.6) and (2.7).
- Periodic conditions are defined in Eq. (2.29h) using a base period t_p and the number of repetitions, N.

User-adjustable periodic conditions can be modified according on the availability of price signals, the relevant time horizon, and additional parameters.

Moreover, an optimization model shown in Figure 2.2 is built to highlight the relationships among several problem components. Its components are explained in Table 2.2. As thoroughly reported in mathematical optimization literature [39], the choice of units can negatively influence problem scaling and lower its efficacy. By carefully altering the order of magnitude of problem parts, one may generate a computationally favored problem, therefore avoiding unstable and ineffective algorithmic computations [40]. Solving the case studies in this thesis without suitable

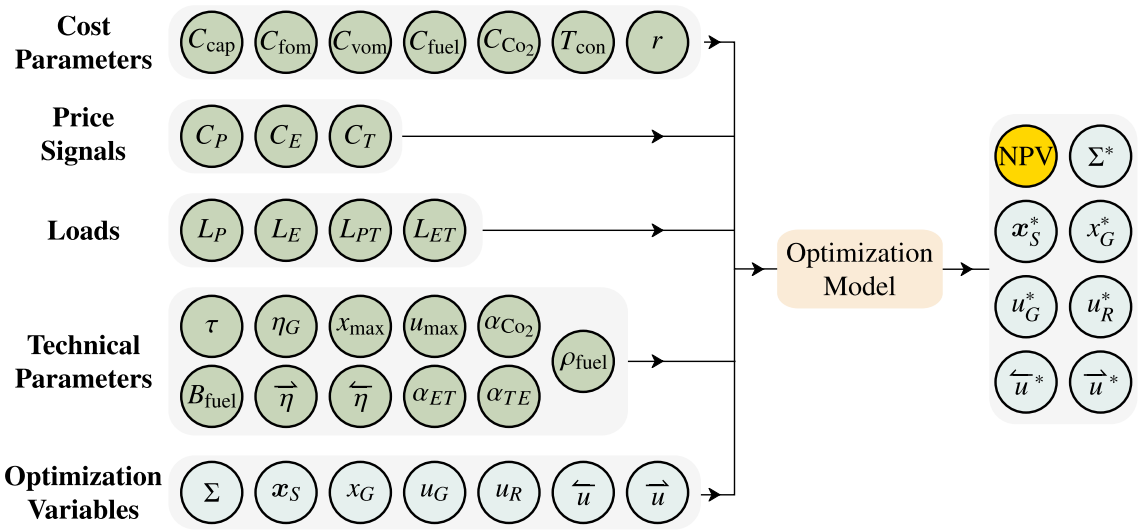

Figure 2.2: Optimization model with inputs and outputs

scaling using 10^{-6} solver tolerance, for instance, can occupy up to a day of computing effort. This is thus because the optimizer will devote a lot of effort maximizing for 10^{-6}th of a dollar value. From a more general standpoint, it is abundantly evident that 10^{-6}th of a dollar value is negligible during the lifespan of the project, with an NPV value in the millions of dollars. The problem may be solved in less than 280 seconds by applying a scaling factor of 10^9 for the goal function and suitably selected scaling factors for other problem parts, therefore indicating a significant rise in computing efficiency. Reference [40] offers a more thorough review of scaling in dynamic optimization situations.

Table 2.2: Summary of optimization model input and output parameters

Parameter Group	**Symbol**	**Description**
Cost Parameters	C_{cap}	Capital expenditure for system components
	C_{fom}	Fixed operational and maintenance costs
	C_{vom}	Variable operational costs
	C_{fuel}	Fuel costs
	C_{CO_2}	Carbon emission tax
	T_{con}, r	Construction time and discount rate
Price Signals	C_P	Market price of primary energy
	C_E	Electricity market price
	C_T	Price of tertiary product (e.g., hydrogen)
Load Parameters	L_P	Primary energy load
	L_E	Electricity load
	L_{PT}, L_{ET}	Additional loads for tertiary storage
Technical Parameters	η_G	Generator efficiency
	τ	Ramp rate constraints
	$x_{\text{max}}, u_{\text{max}}$	Maximum allowable state and control variables
	α_{CO_2}	CO_2 emission factor
	ρ_{fuel}	Fuel consumption rate
	$\overrightarrow{\eta}, \overleftarrow{\eta}$	Electricity-to-thermal and thermal-to-electric efficiency
	α_{ET}, α_{TE}	Tertiary energy conversion efficiencies
Variables	Σ	Total storage capacity
	x_G, x_S	States of generator and storage
	u_G, u_R	Control decisions for power and revenue
	$\overrightarrow{u}$	Charging control signal
	$\overleftarrow{u}$	Discharging control signal

Chapter 3

Results and Discussion

This section provides several case studies to demonstrate the effectiveness of the proposed framework. These studies are selected to highlight, to the extent possible, different operational modes that employ various technologies and storage types. The common characteristics among these methods are delineated in Table 3.1.

While different time intervals, including minute-by-minute decision-making, can be used as appropriate, this work with ECOGEN-CCD defaults to an hourly time mesh inside DTQP. The zero-order hold strategy is suitable during these periods as the control decisions are piecewise constant, and so there is no discretization error for the state dynamics. Then, the dynamic optimization problem is discretized via direct transcription using an equidistant mesh and a composite Euler forward quadrature method. Based on the current assumptions described in the previous section, the resulting capacity and dispatch optimization problem becomes a linear optimization problem. Using `MATLAB`'s linprog optimization solver, the convexity feature of the problem may be efficiently handled for the global optimal solution; although, given the problem matrices from DTQP, different solvers may be used. linprog used a solver tolerance of 10^{-9} using the dual-simplex-highs algorithm. A single desktop workstation with an AMD Ryzen 9 3900X 12-core processor at 3.79 GHz, 32 GB of RAM, 64-bit Windows 10 Enterprise LTSC version 1809, and `Matlab` R2024a was used to obtain the results.

Table 3.1: Cost parameters for generator and storage technologies used in Case Study I, II, and III

Parameters	Generator				Storage				
	Capital Cost	Wind	Nuclear	Unit	TES	BESS	Unit	Hydrogen	Unit
Nominal capacity	1083	200	2156	MW	-	50	MW	640	tpd
C_{occ}	0	1.265M	6.041M	\$/MW	1.049M	347k	\$/MWh	600.074	\$/kg
C_{fom}	12.2k	26.34k	121.64k	\$/MW-yr	4.79	0.718	\$/MWh-h	0	\$/kg-yr
C_{vom}	1.87	0	2.37	\$/MWh	0.75	0	\$/MWh	0.288	\$/kg

3.1 Natural Gas Combined Cycle with Thermal Energy Storage and Carbon Capture and Storage

Using CCS technology, fossil fuel-based generators, including NGCC power plants, are considering a reduction in carbon emissions in line with projected environmental laws. The addition of a CCS reduces net plant efficiency and power output, therefore increasing energy prices [41]. As discussed in [26,42], integrating the system with a thermal energy storage (TES) offers a workable mitigation strategy.

This study assumes that the current NGCC power plant, already built and equipped with a CCS unit (thus saving overnight building expenses), will be updated to include a TES system. The CCS only operates during the plant's running state. Specified as a predetermined percentage of the generator's power output, the CCS function is defined by a thermal and electrical load required for the operation of the CCS unit. As such, these electrical and thermal loads show up in the problem and need to be taken care of each time the generator runs. Including a hot thermal storage unit in the design lets operators efficiently remove certain parasitic thermal loads from the power plant during times of high energy prices, therefore maximizing profits. The investigated system is shown in Figure 3.1, and specific technology-dependent parameters are shown in Table 3.2.

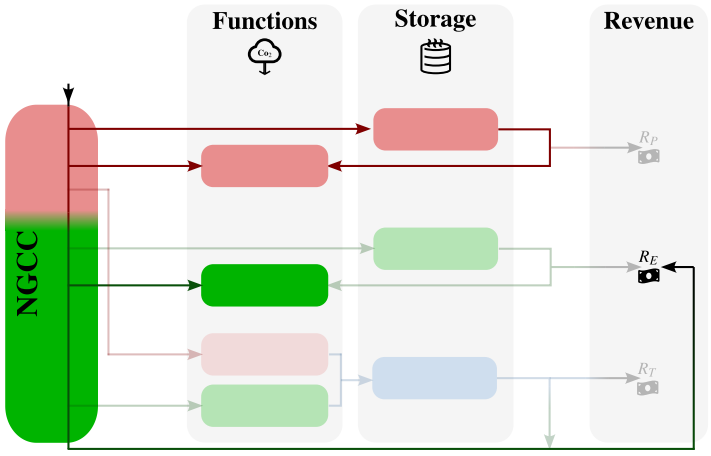

Figure 3.1: IES candidate for Case Study I: A natural gas combined cycle power plant with thermal storage and a carbon capture and storage system. The section colored pink and green illustrates the primary energy domain and the electrical domain, respectively.

Table 3.2: Parameters associated with Case Study I for an NGCC generator with CCS and a TES largely based on [26]

Field	Value	Unit	Field	Value	Unit
ρ_{fuel}	146.952	kg/h MW	α_{CO_2}	0.0029	ton/kg
τ	0.1389	h	η_G	1	–
$u_{G,\min}$	0	MW	$u_{G,\max}$	1083	MW
$x_{G,\min}$	0	MW	$x_{G,\max}$	1083	MW
$x_S(t_0)$	25	MWh	$x_S(t_f)$	25	MWh
$\overrightarrow{u}_{\max}$	200	MW	$\overleftarrow{u}_{\max}$	200	MW
L_P	$0.1x_G$	MW	L_E	$0.2x_G$	MW
T_{con}	3	years	r	0.075	–

Using an hourly time mesh encompassing 262,980 time grid points, this problem is investigated over a 30-year operational period. It is hypothesised that thermal energy cannot be directly sold; rather, it may only be used to supply the thermal load demand from CCS. Tables 3.1 and 3.2 illustrate the main derived input parameters for this case study, largely obtained from [26, 43].

A globally optimal solution is effectively obtained in only 1000 [s] thanks to linearity and convexity. The results of this case study are expanded upon below and shown in Figures 3.2.

Closely related to the cost of electricity and fuel is the performance of the proposed generator and storage system in the optimization problem. First, a two-year period of the full 30 years is shown in Figure 3.3, including generator discharge, storage use, and power exported to the grid under varying electricity price conditions. The findings are examined for a designated period between hours 580 to 620 taken from the larger simulation horizon shown in Figure 3.2, thereby enabling a more detailed study of the system behavior.

Figure 3.2 highlights two time periods where: ① corresponds to low electricity prices and ② is associated with high electricity prices. Accordingly, as illustrated in Figure 3.2a, electricity prices are low in the area defined by ①, so using the generator is generally unprofitable. Nevertheless, as Figure 3.2b shows, this period ① offers the generator a good opportunity to charge the storage unit. Figures 3.2c show the charge and discharge signals during this period. As seen in Figure 3.2d, the electricity sold to the grid during ① is zero.

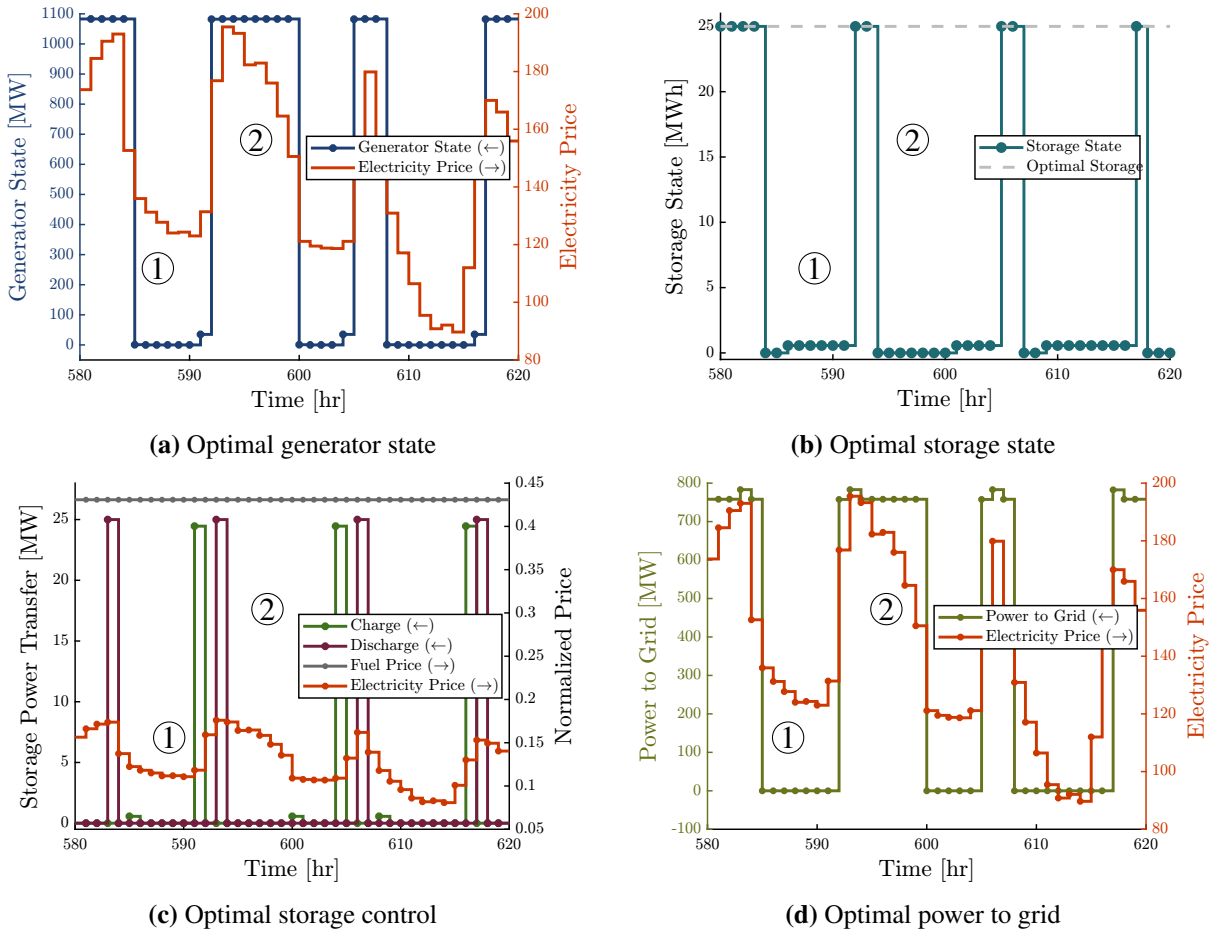

(a) Optimal generator state

(b) Optimal storage state

(c) Optimal storage control

(d) Optimal power to grid

Figure 3.2: Case Study I: Optimal state and control variables for NGCC generator with TES and CCS

Conversely, the period ② shows how the system responds to a scenario whereby the electricity prices are really high. Running the generator at full or high capacity during this period is advantageous (see Figure 3.2a). High power prices also drive the discharge of stored energy during this period, per Figures 3.2b and 3.2c. In this phase, the released thermal energy removes the generator's thermal load to CCS, therefore enabling a rise in output of electricity to the grid. This is illustrated in Figure 3.2d.

Overall, the optimal storage capacity is found to be 25 [MWh], and the NPV is -1.07×10^9 [$]. These results rely on several critical assumptions that should be reconsidered to evaluate a specific site location. Additionally, current historical market signals were derived from [44, 45], but including predicted future market signals (e.g., from [46, 47]) could assist in the decision-making process by evaluating the prospective grid composition and climate change. Even with these cur-

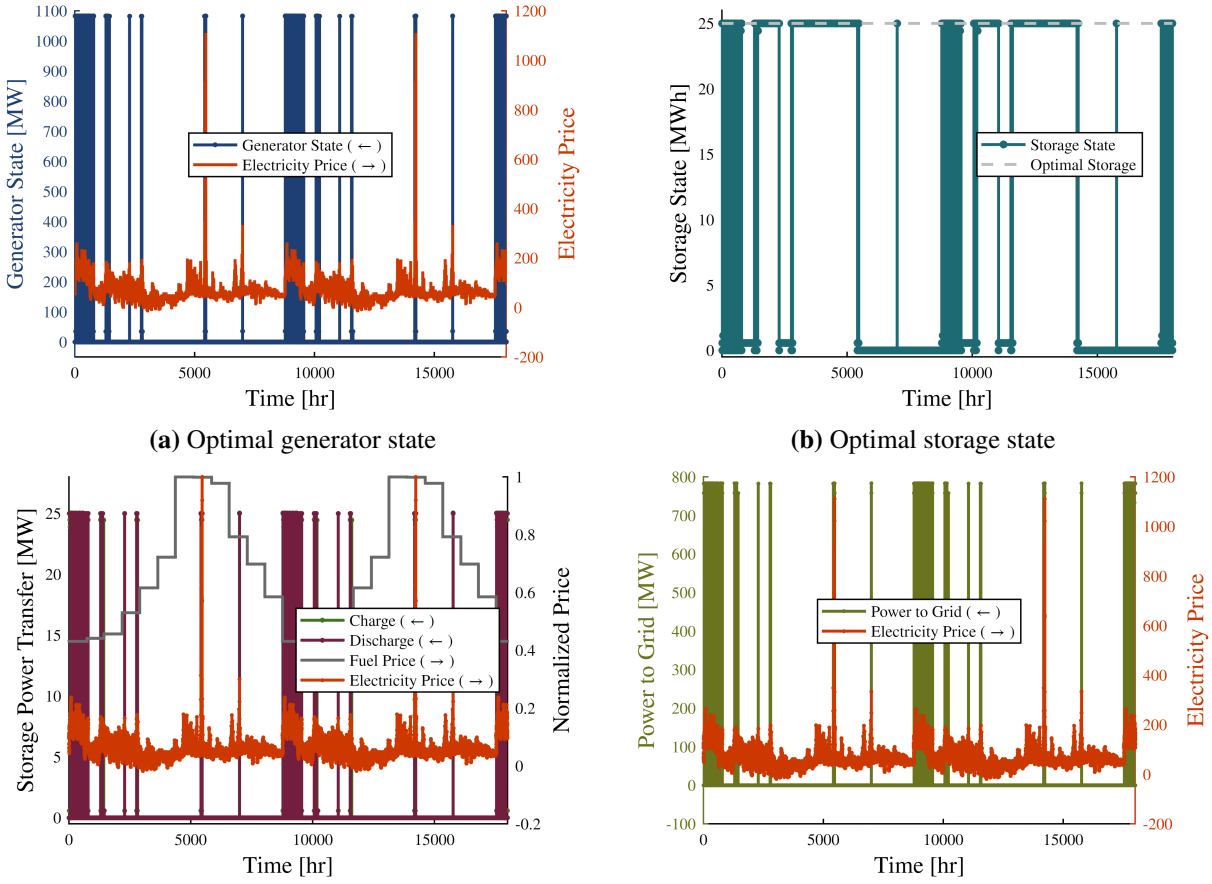

(a) Optimal generator state

(b) Optimal storage state

(c) Optimal storage control

(d) Optimal power to grid

Figure 3.3: Case Study I: Results over the first 2-year period

rent assumptions, the expected trends are observed, and ECOGEN-CCD can be used as a strong framework for the early-stage investigation of these generator and storage technologies. Evaluating the distribution of many functions and requirements across the plant's lifespan might provide insights into its optimal performance. Specifically, Figure 3.4 shows how the energy produced by the generator is utilized. Specifically, 70% of the generator energy is sold to the electricity grid, while 20%, 0.43%, and 9.57% are used for electric load, charge, and primary load, respectively. The relatively small share of the generator in satisfying the primary load is made possible through the inclusion of the thermal energy system, which is responsible for satisfying 95.7% of the thermal energy demand from CCS according to Figure 3.4b. As shown in Figure 3.4c, the storage system is responsible for about 0.695% of the overall revenue.

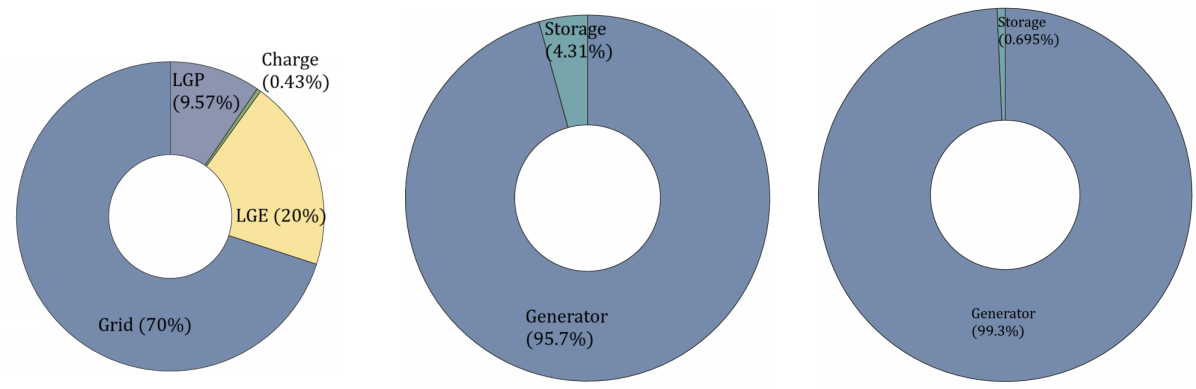

(a) Generator energy **(b)** Primary load **(c)** Revenue

Figure 3.4: Breakdown of various elements in Case Study I: (a) Generator energy usage, (b) Primary load contributions, and (c) Revenue contributions

3.2 Wind Farm with a Battery Energy Storage System

In this case study, we examine an on-shore wind farm with a sizable plant footprint running at 200 [MW] in the Great Plains area together with a 50 [MW] battery storage. The wind farm parameters are based on an example with 71 wind turbines and a nominal capacity of $p_{\text{rated}} = 2.8$ [MW] with a rotor diameter of $D = 125$ [m] and a hub height of 90 [m] [43]. Variations in wind speed produce variations in the power output generated for the grid, thereby compromising the stability and quality of power. Consequently, a BESS is required to reduce these negative effects [48]. High power density and energy efficiency of lithium-ion batteries make them an interesting energy storage method for wind farms [49]. Thus, here is into consideration a utility-scale lithium-ion battery including 25 modular, prefabricated battery storage container structures [43].

Here, the operator can request a specific power output from the generator, and the wind farm operation is primarily determined by the availability of wind. Using wind speed $v_w(t)$ as an additional time-dependent input to the model, the upper bound of Eq. (2.13) was estimated for each turbine based on the wind speeds, wind farm specifications, and the capacity factor of $c_p = 0.55$:

$$p_w = c_p \frac{1}{2} \rho_{air} \frac{\pi D^2}{4} v_w(t)^3 \tag{3.1}$$

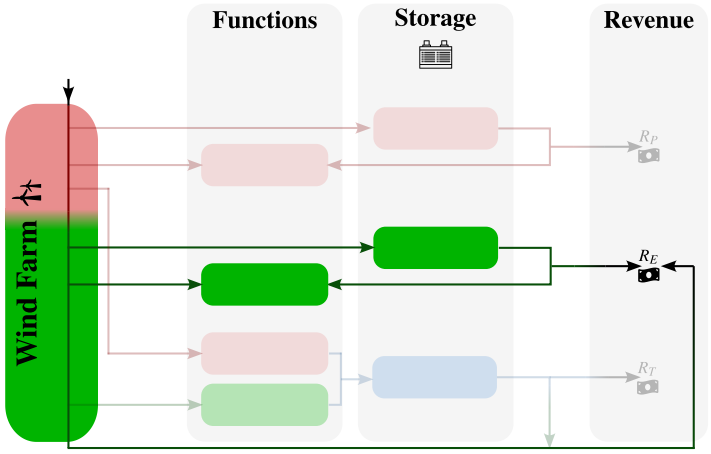

Figure 3.5: IES candidate for Case Study II: A wind farm with a battery energy storage system

Table 3.3: Parameters associated with Case Study II for a wind farm connected to a battery energy storage system, largely based on Ref. [43]

Field	Value	Unit	Field	Value	Unit
ρ_{fuel}	0	kg/h MW	α_{CO_2}	0	ton/kg
τ	0	h	η_G	1	-
$u_{G,\min}$	0	MW	$u_{G,\max}$	200	MW
$x_{G,\min}$	0	MW	$x_{G,\max}$	200	MW
$x_S(t_0)$	15	MWh	$x_S(t_f)$	15	MWh
$\overrightarrow{u}_{\max}$	50	MW	$\overleftarrow{u}_{\max}$	50	MW
L_P	0	MW	L_E	$0.1x_G$	MW
T_{con}	5	years	r	0.075	-

where p_w is the wind power, and ρ_{air} is the air density. The maximum wind power is assumed to happen at $v_w = 25$ [m/s], and the turbine is off for wind speeds above this value. All of the power vector elements greater than p_{rated} are saturated at this value. Finally, the available power output takes into consideration the number of wind turbines in the farm.

Tables 3.1 and 3.3 list the input values related to this case study. Figure 3.5 shows the proposed system whereby the necessity to run auxiliary equipment in the facility results in an electrical load.

Figure 3.7 shows the first two years of the study, including generator discharge, storage utilization, and power exported to the grid under different electricity pricing circumstances.

Unlike in the previous scenario, the availability of wind and wind turbine characteristics mostly determines the generator power level here. Consequently, the generator in Figure 3.6a gathers all

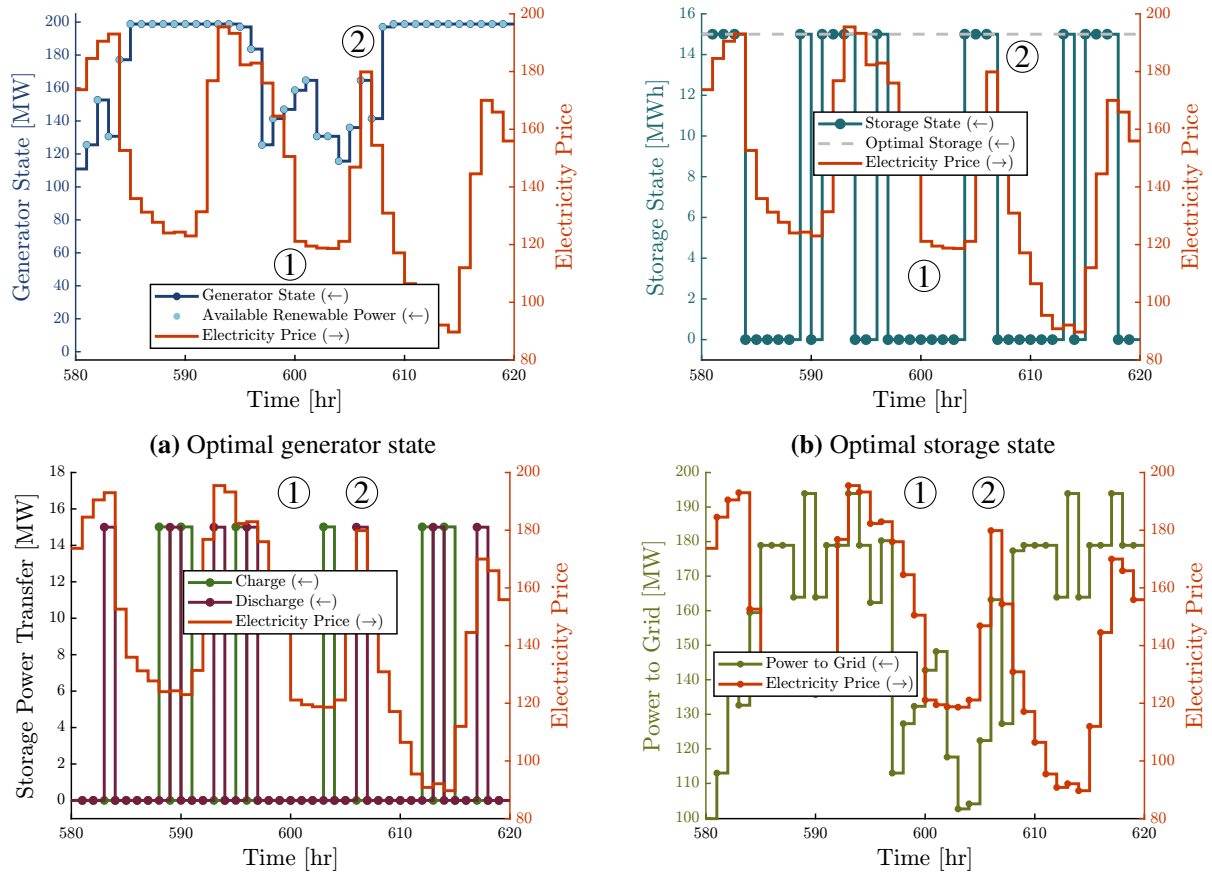

(a) Optimal generator state

(b) Optimal storage state

(c) Optimal storage control

(d) Optimal power to the grid

Figure 3.6: Case Study II: Optimal state and control variables for a wind farm with a battery storage unit

the wind power for which it is suitable. Conversely, the choices on charge and discharge are mostly influenced by the cost of electricity. Figure 3.6c makes it abundantly evident that the charge signal lowers and the discharge signal rises under high-electricity pricing. As seen by region ①, in Figures 3.6b and 3.6c, this causes very substantial decreases in the storage state. The power sold to the grid stays very low, as the wind power accessible in this period is slightly less than that of the surrounding time periods (Figure 3.6). This is seen in Figure 3.6d.

The NPV is 0.80×10^9 [$], showing that for a sizable wind farm, a utility-scale BESS has the potential to be economically competitive. The optimal storage capacity is 15 [MWh]. Figure 3.8 displays the percentages related to the energy generated by the generator and the shares of the generator and storage unit from the electrical load and income. Accordingly, 1.18% of the generated

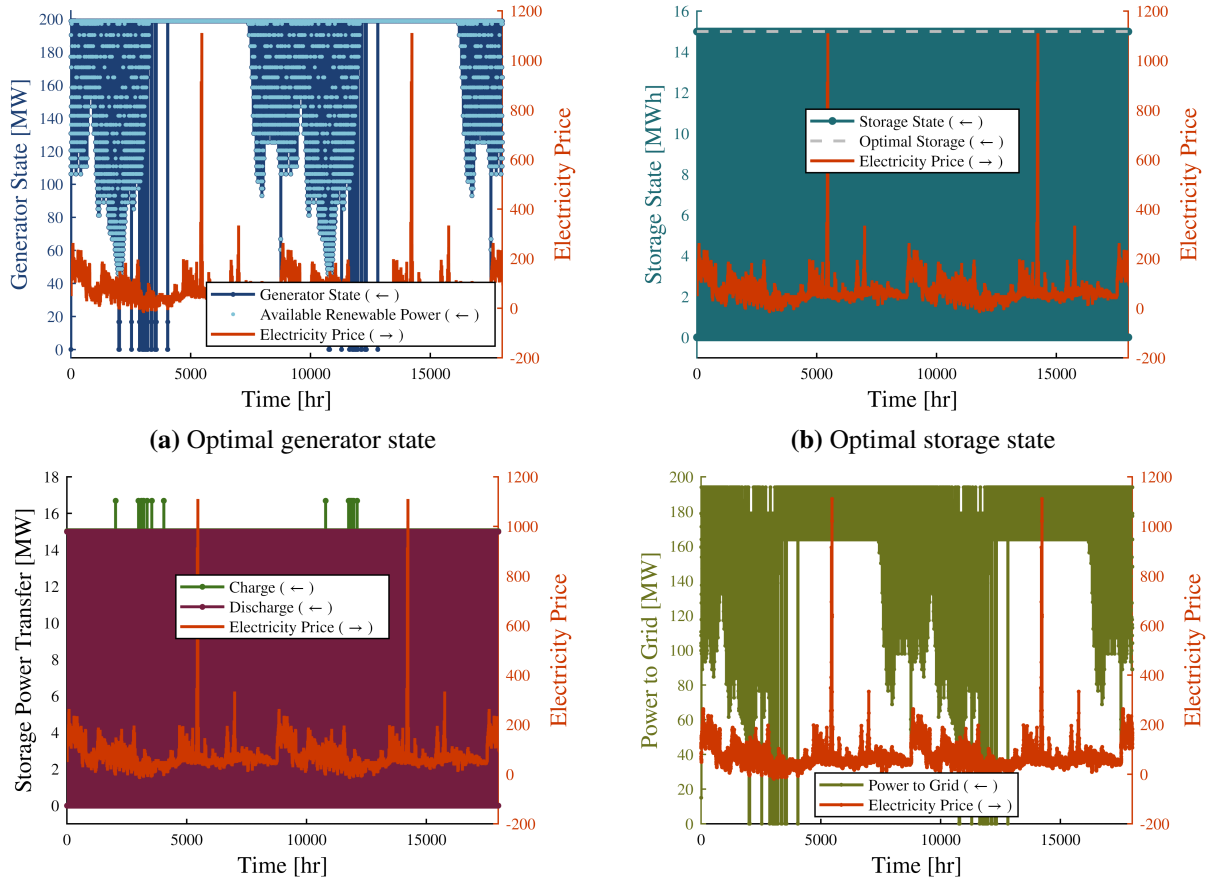

(a) Optimal generator state

(b) Optimal storage state

(c) Optimal storage control

(d) Optimal power to grid

Figure 3.7: Case Study II: Results over the first 2-year period

energy is used to charge the BESS, while 8.88% is used to satisfy the electric load demands. Over the project's life, the storage will satisfy 11.2% of this load demand, and the generator will satisfy the remainder. Finally, generator contributions to the revenue are estimated as 98.4%.

3.3 Nuclear Power Plant with Hydrogen Production and Storage

Since they are one of the energy sources with low carbon emissions after hydropower, nuclear power plants (NPPs) are increasingly important in the future of the electrical industry [50]. Still, low power prices from other generating sources, as well as other complications, call for their economic sustainability to be questioned. Conversely, the hydrogen market has grown remarkably

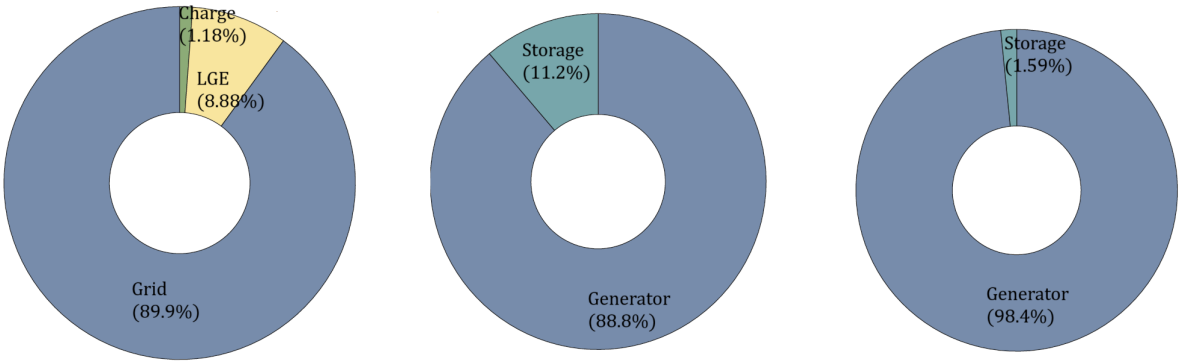

(a) Generator energy **(b)** Electrical load **(c)** Revenue

Figure 3.8: Breakdown of various elements in Case Study II: (a) Generator energy usage, (b) Electrical load contributions, and (c) Revenue contributions

both in the United States and internationally, more than threefold since 1975 [51]. The expanding market for hydrogen presents a unique opportunity for NPPs to enter other markets, as the integration of NPPs with other markets and technologies has the potential to maintain NPPs' competitiveness [4,52,53]. This case study, shown in Figure 3.9, examines how NPP may be integrated with a hydrogen facility and storage. This hybrid operation [53] enables them to strategically (depending on economics) generate hydrogen or sell power to the grid, therefore releasing NPPs from their conventional baseload. Here we investigate an NPP with two pressurized water reactors (PWR), whereby the heat produced by the fuel in the reactor is expelled into the surrounding pressurized cooling water.

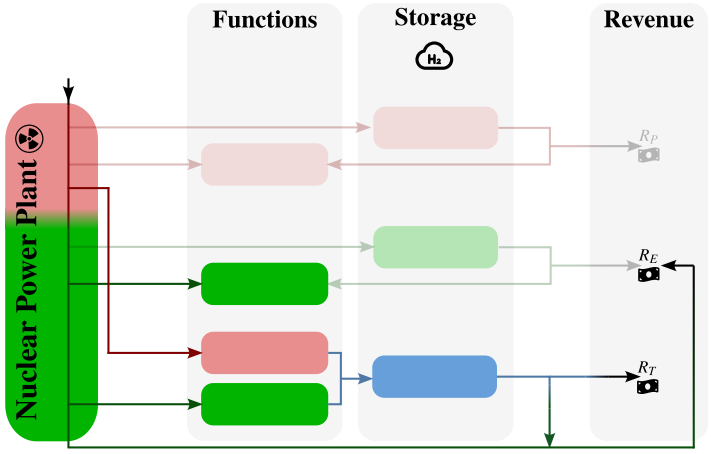

Figure 3.9: IES candidate for Case Study III: A nuclear power plant with hydrogen production and storage

Table 3.4: Parameters associated with Case Study III for a nuclear power plant connected to a hydrogen production and storage facility, largely based on Refs. [43, 52, 53, 57, 58]

Field	Value	Unit	Field	Value	Unit
ρ_{fuel}	0.001	kg/h MW	α_{CO_2}	0	ton/kg
τ	1.79	s	η_G	1	-
$u_{G,\text{min}}$	0	MW	$u_{G,\text{max}}$	2156	MW
$x_{G,\text{min}}$	0	MW	$x_{G,\text{max}}$	2156	MW
$x_S(t_0)$	500	kg	$x_S(t_f)$	500	kg
$\overrightarrow{u}_{\text{max}}$	1065	MW	$\overleftarrow{u}_{\text{max}}$	27990	kg/h
L_P	$0.1\,\overrightarrow{u}$	MW	L_E	$0.1x_G$	MW
T_{con}	7	years	r	0.075	-
α_{ET}	0.0377	MWh/kg	α_{TE}	29.762	kg/MWh

After passing through a steam generator, the pressurized water absorbs the heat without boiling and then runs through a steam turbine to create energy. Using the high-temperature steam electrolysis (HTSE) technique [54], hydrogen is generated, requiring both thermal and electrical connections to the NPP. This work assumes that for every unit of power, 10% thermal energy is needed to generate hydrogen based on load requirements recorded in [53]. The thermal demand is then established as a function of the input electricity from the tertiary charging signal, therefore guaranteeing that the thermal loads are only present when a choice to manufacture hydrogen is taken. While hydrogen market prices are assumed to be set at 7.0 [$/kg] of hydrogen, which is inside the price range provided in [55], the cost of the fuel is created based on projections published in [56]. Mostly based on [43, 53], the cost parameters for the NPP and the hydrogen generation and storage facilities are shown in Table 3.1. Table 3.4 shows the remaining problem parameters.

Under the following constraint, informed by hydrogen market operations and the reality that sales of hydrogen may only occur at prescheduled periods, this case study addresses a discrete daily demand:

$$\mathbf{0} \leq \boldsymbol{u}_{TR}(t) \leq \begin{cases} \boldsymbol{u}_{\text{max}}, & \text{if } t = 8 \text{ AM} \\ \mathbf{0}, & \text{otherwise} \end{cases} \tag{3.2}$$

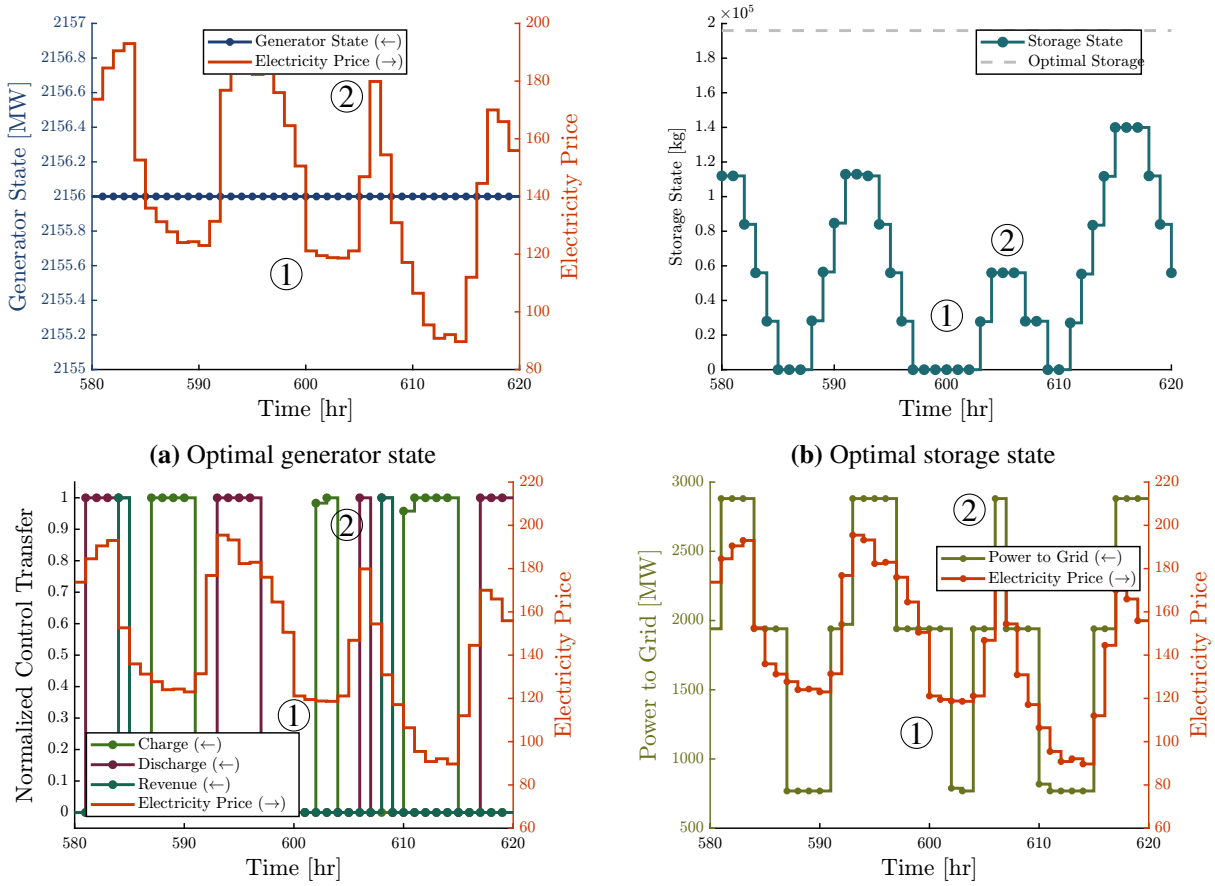

(a) Optimal generator state

(b) Optimal storage state

(c) Optimal storage control

(d) Optimal power to grid

Figure 3.10: Case Study III: Optimal state and control variables for a nuclear power plant with a hydrogen production and storage facility

According to this equation, hydrogen sales can only occur between $8-9$ AM on a daily basis.

Figure 3.10 shows the zoomed-in results after 30 years of operation. Figures 3.10a show that the NPP power level remains at the maximum level over both periods when electricity prices are low ① and when they are high ②. As shown by Figure 3.10b, the level of hydrogen storage rises and falls correspondingly depending on period ① and ②. Direct sales of hydrogen, which become feasible daily between 8–9 AM, produce a periodic discharge of hydrogen, in which most of the discharged hydrogen is directly sold to the market, per Figure 3.10c.

The power sold to the grid is shown in Figure 3.10d, where it is evident that the power sold to the grid is high in region ② when the electricity prices are high.

(a) Generator energy

(b) Revenue

Figure 3.11: Breakdown of various elements in Case Study III: (a) Generator energy usage, and (b) Revenue contributions

The optimal storage capacity is 195930 [kg], with the NPV of -2.94×10^9 [$], indicating that under current assumptions, including retail prices, facility costs, and lifetime of the facility, the project needs further time to become profitable. Figure 3.11a indicates that from the total generator's energy, 78.7% was directly sold to the electricity grid, while 10.2% was used for charging the tertiary hydrogen storage, 10% was used to satisfy auxiliary electrical loads[1], and 1.02% was used to satisfy the primary load demand for HTSE. In this case study and with the presented assumptions, the storage is responsible for 7.48% of the generated revenue over the lifetime of the project. This result is shown in Figure 3.11b.

Based on [59], 60% to 70% of the cost of power produced by NPPs is directly related to capital costs. Since NPPs are characterized by large capital investments, the consideration of potential uncertainties in overnight construction costs can inform project management, planning, and scheduling. It can also provide unique opportunities for understanding risks — informing further actions to protect investors [38].

[1]Current results assume these auxiliary electrical loads can be met by the NPP itself, which is generally not the case.

3.4 Sensitivity Analysis Results

3.4.1 Implementation of Sensitivity Analysis in ECOGEN-CCD

A fundamental analytical tool used to identify how variations in input parameters (parameters and variables) affect the outputs of a model or system is sensitivity analysis. A sensitivity analysis is performed to evaluate the economic feasibility and resilience of integrated energy system topologies under different technological and financial settings. This study investigates how important input parameters in Figure 2.2, including carbon tax rates, fuel costs (e.g., natural gas), electricity prices, and capital costs associated with both generators and storage technologies, impact the objective function of the ECOGEN-CCD optimization model. Important determinants of system performance and profitability are found by methodically perturbing key inputs, hence guiding improved design, investment, and policy decisions.

Sensitivity studies, which involve methodically scaling each input over a wide range, help evaluate the impact of key cost factors on system performance. Particularly, three storage-related cost components — fixed O&M, variable O&M, and overnight capital cost — are individually changed as well as the generator's capital cost and variable O&M. Every parameter is varied across 50 values, logarithmically spaced between 10% and 300% of its starting value. This amounts to a relative shift of -90% to $+200\%$, therefore covering both major price escalations and cost-cutting situations. This method enables a thorough investigation into how variations from nominal values impact optimal storage size and NPV, thereby revealing information on the cost sensitivity and economic resilience of the system.

3.4.2 Sensitivity Analysis of Case Study I

With a focus on energy use and generator and TES income contributions, a sensitivity study was done to evaluate how different the carbon tax rate affected system performance. The basic solution is a carbon tax of 65 [$\$/\text{ton}$]; other scenarios show variations around this nominal value. Generator energy use is constant at 70% of system operation, with 20% allocated to fulfill electrical

Table 3.5: Case Study I: Impact of carbon tax on system's optimal NPV and operational metrics with carbon tax of 65 [$/ton] is considered for optimal case

Carbon Tax	Gen Energy %	LGE %	Charge %	LGP %	Gen Prim %	Storage Prim %	Gen Rev %	Storage Rev %	NPV ($\times 10^9$)
0	70	20	0.373	9.63	96.3.1	3.73	99.4	0.594	-1.138
15	70	20	0.36	9.64	96.4	3.59	99.4	0.594	-1.148
25	70	20	0.377	9.62	96.2	3.77	99.4	0.61	-1.155
35	70	20	0.388	9.61	96.1	3.87	99.4	0.624	-1.606
45	70	20	0.418	9.58	95.8	4.17	99.3	0.664	-1.165
55	70	20	0.415	9.59	95.9	4.15	99.3	0.668	-1.169
65	**70**	**20**	**0.432**	**9.57**	**95.7**	**4.31**	**99.3**	**0.695**	**-1.173**
70	70	20	0.449	9.55	95.5	4.49	99.3	0.722	-1.175
75	70	20	0.449	9.55	95.5	4.49	99.3	0.722	-1.176
80	70	20	0.491	9.51	95.1	4.9	99.2	0.775	-1.177
85	70	20	0.509	9.49	94.9	5.09	99.2	0.799	-1.179
90	70	20	0.521	9.48	94.8	5.2	99.2	0.816	-1.180
95	70	20	0.555	9.45	94.5	5.54	99.1	0.86	-1.183
100	70	20	0.548	9.45	94.5	5.47	99.1	0.855	-1.183
105	70	20	0.565	9.44	94.4	5.64	99.1	0.877	-1.187
110	70	20	0.58	9.42	94.2	5.8	99.1	0.9	-1.188
150	70	20	0.593	9.41	94.1	5.93	99.0	0.994	-1.189
200	70	20	0.732	9.27	92.7	7.31	98.8	1.16	-1.189
250	70	20	0.856	9.14	91.4	8.55	98.7	1.3	-1.190
300	70	20	0.654	9.35	93.5	6.54	98.8	1.21	-1.190
350	70	20	0.762	9.24	92.4	7.61	98.7	1.31	-1.190

load needs, as stated in Table 3.5 and visually shown in Figure 3.12. These figures show the generator runs constantly throughout the carbon cost spectrum, not sensitivity to carbon pricing.

While the fraction of generator energy allocated to direct primary thermal load shows a minor decrease as the carbon tax rises from 15 to 300 [$/ton], the TES charging activity increases gradually from 0.373% to 0.762% to fulfill CCS thermal demands, thus improving the emission cost efficiency. The breakdown of primary load satisfaction supports this trend: the TES share increases from 3.73% to 7.61%, and the generator's contribution lowers in line with the system's aim of reducing on-site combustion under more strict carbon pricing scenarios. Likewise, the revenue distribution shows this change as TES's share rises modestly from 0.594% to 1.31% with increasing carbon taxes, so highlighting its increasing importance in reducing the operational load of the generator and increasing profitability; conversely, the generator's revenue share somewhat declines from 99.4% to 98.7%, consistent with this change.

Reflecting a notable decrease in project profitability under tougher emissions penalties, the Net Present Value falls gradually with rising carbon tax as seen in Figure 3.12, going from -1.138×10^9 [$] at 0 [$/ton] to -1.190×10^9 [$] at 350 [$/ton].

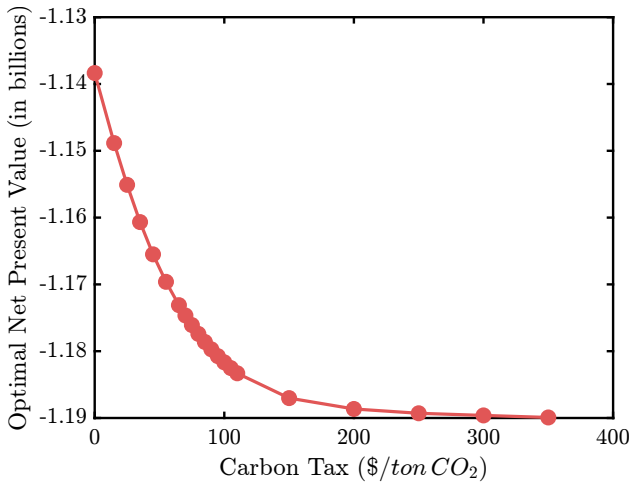

Figure 3.12: Case Study I: Optimal net present value under varying carbon tax rates

Figure 3.13 shows, in Case Study I, the temporal behavior of generator output and storage control signals over four carbon tax levels. Reflecting the growing economic penalty on emissions-intensive generation, generator dispatch clearly shows a decrease in both frequency and amplitude as the carbon tax rises from 25 to 300 [$/ton]. While at 300 [$/ton] its utilization is significantly decreased, matching with lower cost-effectiveness of fossil-based production, at low tax levels (e.g., 25 [$/ton]) the generator runs often and at high output levels. It should be noted that optimal storage across various carbon tax values for this case study does not change and exactly matches the baseline case where 65 [$/ton] carbon tax value is considered.

Still, the related storage activity shows a non-monotonic pattern. Storage shows both active charging and discharging at lower tax levels (25 and 65 [$/ton]), with discharge events timing with periods of high electricity prices. Discharge intensity lowers at an intermediate tax level (200 [$/ton]), goes almost zero as the carbon tax value gets its 300 [$/ton] value.

This nonlinear response of storage emphasizes the intricate interaction of generator economics, carbon price, and signals of the power market. Although increasing carbon taxes methodically reduces generator output, the temporal structure and volatility of energy prices define the behavior of the storage system, in addition to the possibility of avoiding generating expenses.

Benchmarked against a reference "Optimal", Table 3.6 shows the best system outputs under eight distinct scenarios of natural gas price multipliers ranging from 0.0001 to 0.0008. Especially,

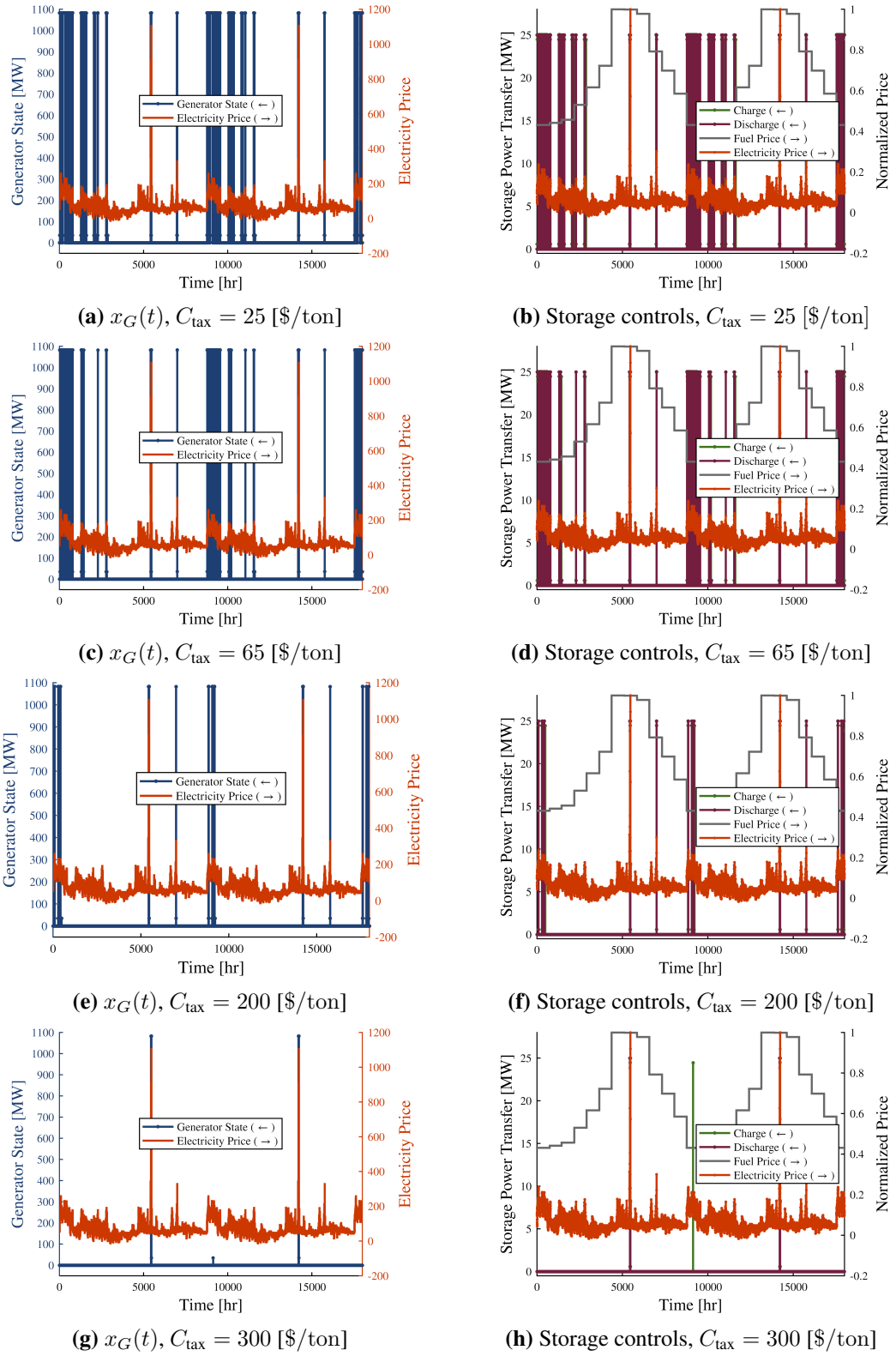

(a) $x_G(t)$, $C_{\text{tax}} = 25$ [\$/ton]

(b) Storage controls, $C_{\text{tax}} = 25$ [\$/ton]

(c) $x_G(t)$, $C_{\text{tax}} = 65$ [\$/ton]

(d) Storage controls, $C_{\text{tax}} = 65$ [\$/ton]

(e) $x_G(t)$, $C_{\text{tax}} = 200$ [\$/ton]

(f) Storage controls, $C_{\text{tax}} = 200$ [\$/ton]

(g) $x_G(t)$, $C_{\text{tax}} = 300$ [\$/ton]

(h) Storage controls, $C_{\text{tax}} = 300$ [\$/ton]

Figure 3.13: Case Study I: Comparison of generator state (left column) and storage control signals (right column) at four carbon tax levels. Carbon tax value of 65 [\$/ton] is considered as a baseline value in this work.

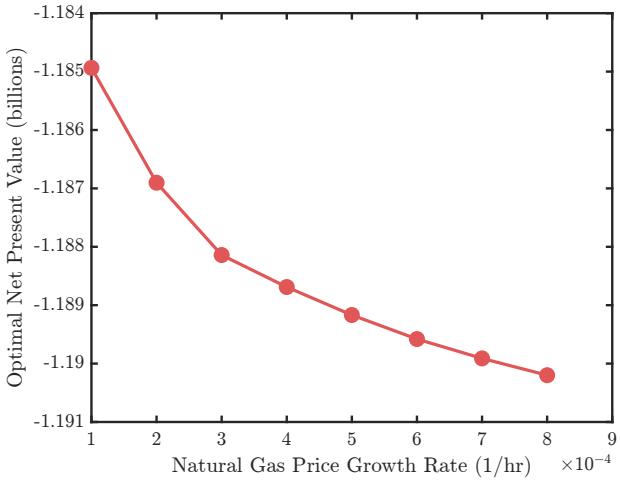

Figure 3.14: Case Study I: Optimal NPV under varying fuel price scenarios

in all scenarios, the generating mix stays constant at 70% Gen Energy and 20% LGE, therefore, confirming system dependence on these sources. On the distribution of charging and LGP components, however, there are small but consistent changes.

Rising natural gas price multipliers provide a slow rise in the fraction of generation focused on storage, as seen in Figure 3.14. Particularly, the *Storage Primary %* increases from 4.21% at a multiplier of 0.0001 to 4.42% at 0.0008, therefore showing a strategy change toward more dependence on storage as fuel costs rise. The distribution of income shows a similar trend, although generating still accounts for over 90% of total revenue, the proportion from storage continuously increases and reaches a high of 0.655% in the mid-range of the multiplier spectrum.

Although all scenarios produce negative Net Present Values (NPVs), the data are nonetheless rather important for assessing financial success. Slightly improving on the baseline of -1.173×10^9 [$], the NPV is least negative at a natural gas price multiplier of 0.0002 (-1.184×10^9 [$]. This suggests small price increases may improve cost-effectiveness. But as the multiplier surpasses 0.0003, NPVs drop dramatically, reaching -1.190×10^9 [$] at 0.0008, probably due in part to greater reliance on costly storage options. These results demonstrate the sensitivity of system economics to fuel pricing and suggest the existence of an ideal pricing range that strikes a balance between environmental goals and financial feasibility.

Table 3.6: Case Study I: Sensitivity of NPV and system metrics for Cases 1 through 8

Case	Gen Energy %	LGE %	Charge %	LGP %	Gen Prim %	Storage Prim %	Gen Rev %	Storage Rev %	NPV
1 (Optimal)	**70**	**20**	**0.421**	**9.58**	**95.8**	**4.21**	**99.3**	**0.718**	**-1.173**
2	70	20	0.438	9.56	95.6	4.38	99.3	0.725	-1.184936
3	70	20	0.439	9.56	95.6	4.39	99.3	0.653	-1.186903
4	70	20	0.439	9.56	95.6	4.38	99.3	0.652	-1.188141
5	70	20	0.448	9.55	95.5	4.48	99.3	0.665	-1.188689
6	70	20	0.475	9.53	95.3	4.75	99.3	0.701	-1.189168
7	70	20	0.446	9.55	95.5	4.45	99.3	0.659	-1.189580
8	70	20	0.442	9.56	95.6	4.42	99.3	0.655	-1.190199

Table 3.7: Case Study I: Sensitivity of NPV and system metrics to varying electricity price multipliers

Multiplier	Gen Energy %	LGE %	Charge %	LGP %	Gen Primary %	Storage Primary %	Gen Revenue %	Storage Revenue %	NPV
1 (Optimal)	**70**	**20**	**0.421**	**9.58**	**95.8**	**4.21**	**99.3**	**0.718**	**-1.173**
1.00E–06	70	20	0.379	9.62	96.2	3.79	99.4	0.608	-1.16
5.00E–05	70	20	0.398	9.6	96	3.98	99.4	0.63	-0.159
7.00E–05	70	20	0.396	9.6	96	3.96	99.4	0.627	-0.159
0.0003	70	20	0.311	9.69	96.9	3.11	99.5	0.453	-0.97
0.0005	70	20	0.267	9.73	97.3	2.67	99.6	0.352	+1.82
0.0007	70	20	0.219	9.78	97.8	2.19	99.8	0.183	16.2

Applying a range of multipliers from 1×10^{-6} to 7×10^{-4} investigated sensitivity to change in the price of electricity. Variations in electricity prices have no appreciable effect on the generator dispatch or storage use behavior at lower multipliers, as Table 3.7 summarizes. With 20% assigned to electrical load and almost 0.421% utilized to charge the thermal energy storage, the generator energy stays stable at 70%. But over 3×10^{-4} electricity price multipliers cause a clear change in system viability.

For smaller multipliers, the NPV stays quite flat at around -1.159×10^{9} [\$]; however, it grows significantly as the growth rate increases. Under higher power market conditions, the NPV approaches 16.2×10^{9} [\$] at a multiplier of 7×10^{-4}, suggesting a significant increase in economic feasibility. Figure 3.15 shows this behavior, where the NPV trajectory transitions from near-constant to exponential growth.

Sensitivity analysis of storage related cost parameters (such as C_{occ}, C_{fom}, and C_{vom}) shows that changing these parameters — individually up to three times their nominal values — does not produce any significant variation in optimal storage capacity or net present value, as seen in Figure 3.16. The economic performance of the system is essentially unaltered, exactly matches the

Table 3.8: Case Study I: Sensitivity of NPV to C_{occ_G} multiplier

C_{occ_G}	NPV (10^9)	C_{occ_G}	NPV (10^9)	C_{occ_G}	NPV (10^9)
0.100	−0.126	0.107	−0.134	0.115	−0.143
0.123	−0.153	0.132	−0.163	0.141	−0.174
0.152	−0.186	0.163	−0.199	0.174	−0.212
0.187	−0.227	0.200	−0.242	0.215	−0.259
0.230	−0.277	0.247	−0.296	0.264	−0.317
0.283	−0.339	0.304	−0.362	0.325	−0.388
0.349	−0.415	0.374	−0.444	0.401	−0.475
0.430	−0.508	0.460	−0.544	0.494	−0.583
0.529	−0.624	0.567	−0.668	0.608	−0.715
0.652	−0.766	0.698	−0.820	0.749	−0.878
0.802	−0.941	0.860	−1.008	0.922	−1.079
0.988	−1.156	1.059	−1.238	1.135	−1.327
1.217	−1.421	1.304	−1.523	1.398	−1.632
1.499	−1.748	1.606	−1.873	1.722	−2.007
1.845	−2.150	1.978	−2.304	2.120	−2.469
2.273	−2.646	2.436	−2.835	2.611	−3.038
2.799	−3.256	3.000	−3.489		

ideal outcomes of Case Study I, suggesting insensitivity to variations unrelated to storage-related expenses within the investigated range.

A sensitivity study on the generator overnight capital cost multiplier ($C_{\text{occ},G}$) was conducted across a broad range of values from 0.10 to 3.00. The NPV demonstrates a strong negative correlation with increasing $C_{\text{occ},G}$, as presented in Table 3.8. As the multiplier increases from 0.10 to 3.00, the NPV declines steeply from -0.126×10^9 to -3.489×10^9 [\$], highlighting the significant economic impact of higher capital investment costs. Relative to the baseline NPV of -1.170×10^9 [\$], the improvement at the lower bound represents an approximate increase of $+89.23\%$, while the deterioration at the upper bound reaches nearly -198.21%. Figure 3.17a illustrates this trend, showing a nearly linear decrease in NPV with rising capital expenditure.

These results highlight the importance of accurate generator capital cost estimation during early-stage design, as decisions concerning $C_{\text{occ},G}$ clearly affect the economic feasibility of the system. Nevertheless, despite the significant impact on NPV, variations in $C_{\text{occ},G}$ have no effect on the optimal storage capacity or dispatch characteristics. As a result, the operational design of the system remains robust under changing generator capital cost assumptions.

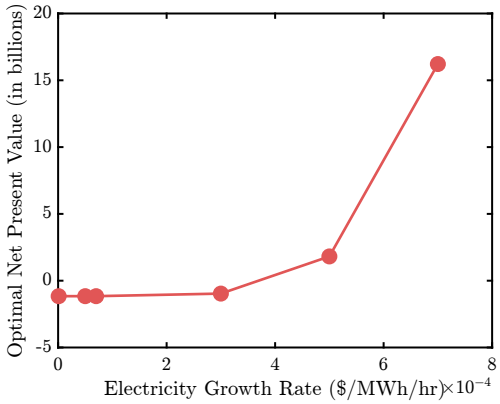

Figure 3.15: Case Study I: Optimal NPV sensitivity to electricity prices

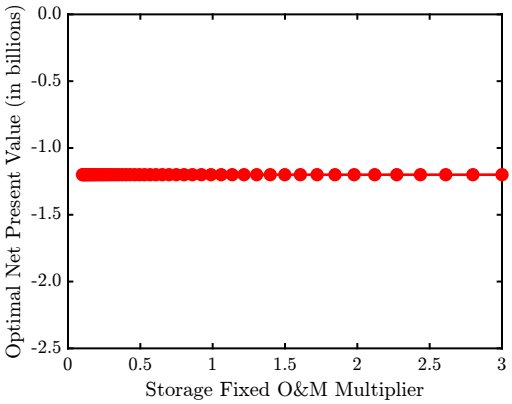

(a) Storage fixed O&M multiplier

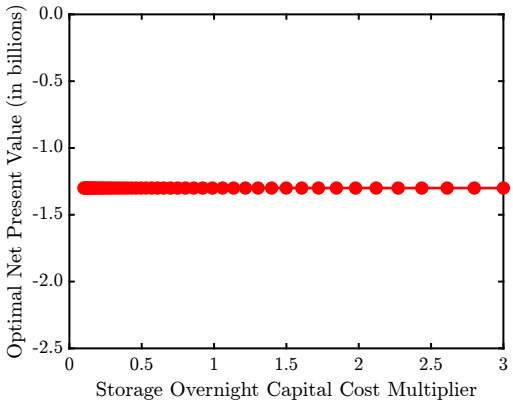

(b) Storage overnight capital cost

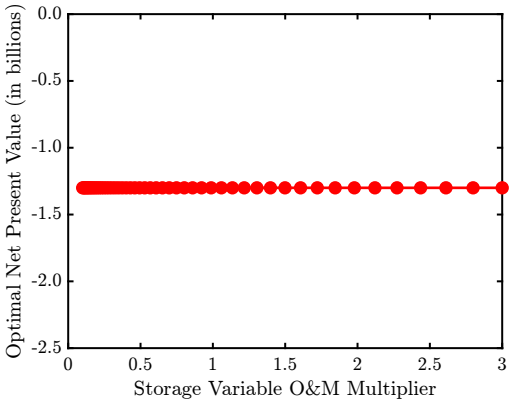

(c) Storage variable O&M multiplier

Figure 3.16: Case Study I: Optimal NPV sensitivity to storage-related cost multipliers

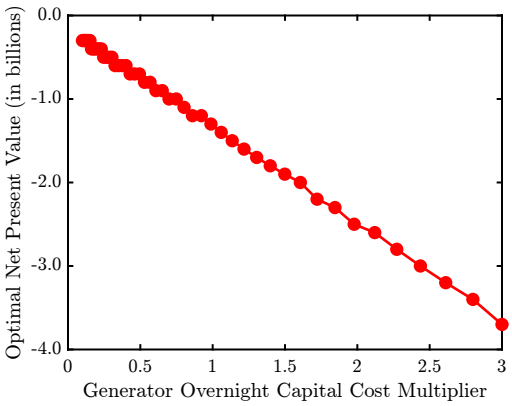

(a) Generator OCC multiplier

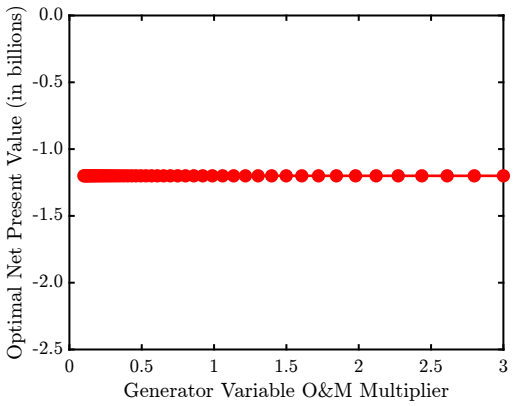

(b) Generator variable O&M multiplier

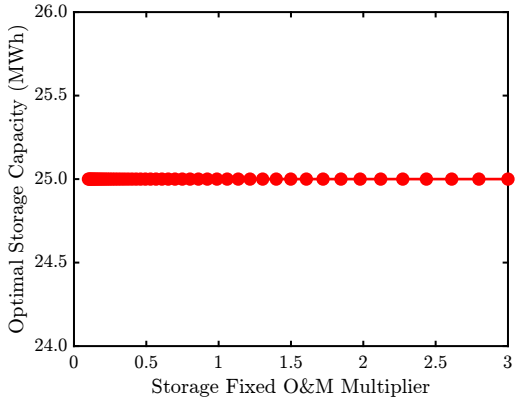

(c) Storage fixed O&M multiplier (capacity)

Figure 3.17: Case Study I: Sensitivity of NPV and optimal storage capacity to generator-related cost multipliers

System economics was assessed throughout the range of 0.10 to 3.00, where each value corresponds to a scalar applied to the nominal variable O&M cost multiplier. Figure 3.17b, shows that for all multiplier values of (C_{vom_G}) the economic performance of the system is tolerant to significant increases in C_{vom_G}.

The ideal storage capacity is not clearly changed by variations in the storage fixed O&M cost multiplier (C_{fom_S}). As Figure 3.17c shows, the storage capacity stays constant at around 25 [MWh] for the whole range of multipliers up to 3.00.

3.4.3 Sensitivity Analysis of Case Study II

As demonstrated in Figure 3.18a, NPV stays constant at 0.14×10^9 [$] across all tested multiplier values, therefore confirming total insensitivity of the system's economic result to changes

in C_{fom_S}. Economic performance is not much affected by variation in the storage overnight capital cost multiplier (C_{occ_S}). With observed values ranging between -0.131×10^9 and -0.132×10^9 [$], NPV varies only slightly around the nominal value of 0.15×10^9 [$], as shown in Table 3.9 and Figure 3.18b. More than 6.5% compared to the baseline, these deviations show no obvious upward or negative trend. The results show that the system is economically robust to fluctuations in storage capital cost under present assumptions. Furthermore, storage size and distribution choices remain untouched by all tested values of C_{occ_S}.

With values ranging between -0.143019×10^9 and -0.143258×10^9 [$], varying the storage variable O&M cost multiplier (C_{vom_S}) results in small and consistent variations in NPV, as illustrated in Table 3.10 and Figure 3.18c. These variations are minor relative to the baseline and show a smooth, monotonic decline in NPV with increasing C_{vom_S}, indicating that system profitability is only weakly sensitive to this parameter.

Increasing the overnight capital cost factor for generators (C_{occ_G}) causes the NPV to slowly and linearly decrease. Table 3.11 and Figure 3.19a show that NPV steadily goes down from 0.163×10^9 [$] at a ratio of 0.10 to 0.158×10^9 [$] at 3.00. The change is minimal — less than 3.07% from the starting value, even though the range is steady. Although C_{occ_G} has a constant effect on project value, the system is economically stable across the range that was tried.

In Case Study II, the generator variable O&M cost multiplier (C_{vom_G}) exhibits a quite unfavorable effect on NPV. NPV falls from around -0.143×10^9 to -0.171×10^9 [$] when the multiplier moves from 0.10 to 3.00 as seen in Table 3.12 and Figure 3.19b. The relationship between C_{vom_G} and optimal NPV is smooth and clearly monotonic, as shown in Figure 3.19b. As the generator variable O&M multiplier increases, the system's profitability steadily declines. This indicates a mild but consistent sensitivity of NPV to changes in C_{vom_G}, with no significant local fluctuations or numerical noise. The results suggest that while increasing generator O&M costs does reduce NPV, the effect is gradual and predictable.

Table 3.9: Case Study II: Sensitivity of NPV to OCC_S multiplier

OCC_S Multiplier	NPV (10^9)	OCC_S Multiplier	NPV (10^9)	OCC_S Multiplier	NPV (10^9)
0.100	−0.131894	0.107	−0.131895	0.115	−0.131896
0.123	−0.131897	0.132	−0.131898	0.141	−0.131899
0.152	−0.131901	0.163	−0.131902	0.174	−0.131903
0.187	−0.131905	0.200	−0.131907	0.215	−0.131908
0.230	−0.131910	0.247	−0.131912	0.264	−0.131915
0.283	−0.131917	0.304	−0.131920	0.325	−0.131922
0.349	−0.131925	0.374	−0.131928	0.401	−0.131932
0.430	−0.131935	0.460	−0.131939	0.494	−0.131943
0.529	−0.131948	0.567	−0.131952	0.608	−0.131957
0.652	−0.131963	0.698	−0.131969	0.749	−0.131975
0.802	−0.131982	0.860	−0.131989	0.922	−0.131997
0.988	−0.132005	1.059	−0.132014	1.135	−0.132023
1.217	−0.132033	1.304	−0.132044	1.398	−0.132056
1.499	−0.132068	1.606	−0.132082	1.722	−0.132096
1.845	−0.132112	1.978	−0.132128	2.120	−0.132146
2.273	−0.132165	2.436	−0.132185	2.611	−0.132207
2.799	−0.132230	3.000	−0.132256		

Table 3.10: Case Study II: Sensitivity of NPV to VOM_S multiplier

VOM_S Multiplier	NPV (10^9)	VOM_S Multiplier	NPV (10^9)	VOM_S Multiplier	NPV (10^9)
0.100	−0.143019	0.107	−0.143020	0.115	−0.143021
0.123	−0.143022	0.132	−0.143023	0.141	−0.143024
0.152	−0.143026	0.163	−0.143027	0.174	−0.143028
0.187	−0.143030	0.200	−0.143031	0.215	−0.143033
0.230	−0.143035	0.247	−0.143036	0.264	−0.143038
0.283	−0.143040	0.304	−0.143043	0.325	−0.143045
0.349	−0.143048	0.374	−0.143050	0.401	−0.143053
0.430	−0.143056	0.460	−0.143059	0.494	−0.143062
0.529	−0.143066	0.567	−0.143070	0.608	−0.143073
0.652	−0.143077	0.698	−0.143082	0.749	−0.143087
0.802	−0.143092	0.860	−0.143097	0.922	−0.143102
0.988	−0.143108	1.059	−0.143114	1.135	−0.143121
1.217	−0.143128	1.304	−0.143135	1.398	−0.143143
1.499	−0.143151	1.606	−0.143159	1.722	−0.143168
1.845	−0.143177	1.978	−0.143187	2.120	−0.143197
2.273	−0.143208	2.436	−0.143220	2.611	−0.143232
2.799	−0.143245	3.000	−0.143258		

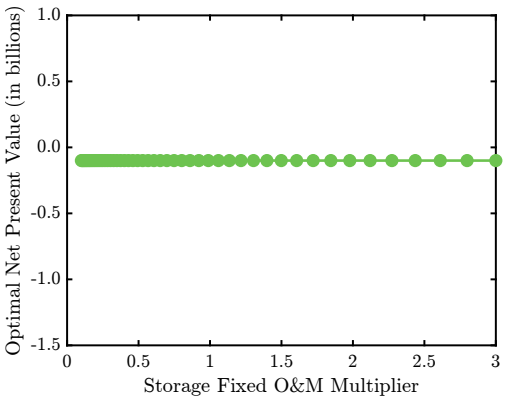

(a) Storage fixed O&M multiplier

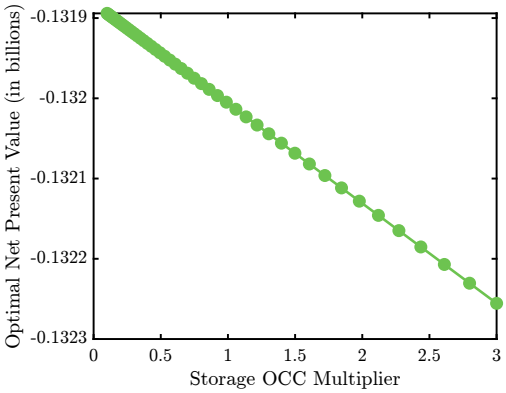

(b) Storage OCC multiplier

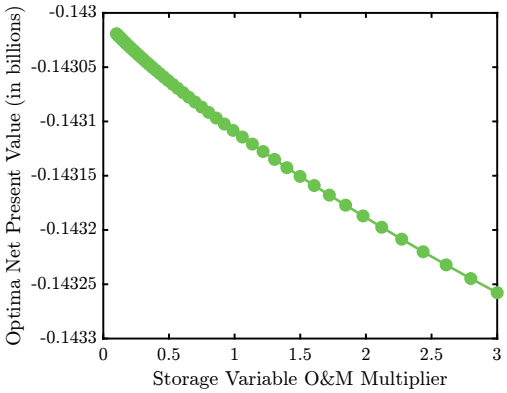

(c) Storage variable O&M multiplier

Figure 3.18: Case Study II: Sensitivity of NPV to storage cost multipliers

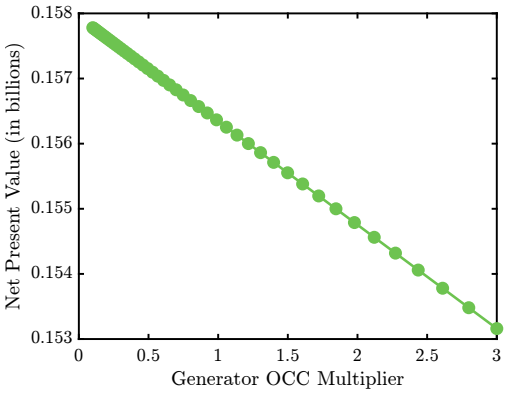

(a) Generator OCC multiplier

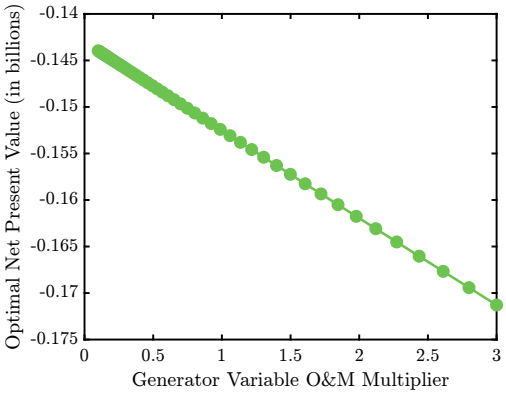

(b) Generator variable O&M multiplier

Figure 3.19: Case Study II: Sensitivity of NPV to generator cost multipliers

Table 3.11: Case Study II: Sensitivity of NPV to C_{occ_G} multiplier

C_{occ_G} **Multiplier**	**NPV (10^9)**	C_{occ_G} **Multiplier**	**NPV (10^9)**	C_{occ_G} **Multiplier**	**NPV (10^9)**
0.100	0.163202	0.107	0.163190	0.115	0.163178
0.123	0.163165	0.132	0.163151	0.141	0.163136
0.152	0.163119	0.163	0.163102	0.174	0.163084
0.187	0.163064	0.200	0.163042	0.215	0.163019
0.230	0.162995	0.247	0.162968	0.264	0.162940
0.283	0.162910	0.304	0.162877	0.325	0.162843
0.349	0.162805	0.374	0.162765	0.401	0.162723
0.430	0.162677	0.460	0.162628	0.494	0.162575
0.529	0.162518	0.567	0.162458	0.608	0.162393
0.652	0.162323	0.698	0.162249	0.749	0.162169
0.802	0.162083	0.860	0.161991	0.922	0.161893
0.988	0.161787	1.059	0.161674	1.135	0.161553
1.217	0.161423	1.304	0.161283	1.398	0.161134
1.499	0.160974	1.606	0.160802	1.722	0.160618
1.845	0.160421	1.978	0.160210	2.120	0.159983
2.273	0.159740	2.436	0.159480	2.611	0.159201
2.799	0.158902	3.000	0.158582		

Table 3.12: Case Study II: Sensitivity of NPV to VOM_G multiplier

VOM_G **Multiplier**	**NPV (10^9)**	VOM_G **Multiplier**	**NPV (10^9)**	VOM_G **Multiplier**	**NPV (10^9)**
0.100	−0.143961	0.107	−0.144030	0.115	−0.144103
0.123	−0.144182	0.132	−0.144267	0.141	−0.144357
0.152	−0.144454	0.163	−0.144558	0.174	−0.144670
0.187	−0.144789	0.200	−0.144917	0.215	−0.145055
0.230	−0.145202	0.247	−0.145359	0.264	−0.145528
0.283	−0.145710	0.304	−0.145904	0.325	−0.146112
0.349	−0.146335	0.374	−0.146573	0.401	−0.146829
0.431	−0.147104	0.460	−0.147398	0.494	−0.147713
0.529	−0.148050	0.567	−0.148412	0.608	−0.148800
0.652	−0.149215	0.698	−0.149660	0.749	−0.150137
0.802	−0.150648	0.860	−0.151195	0.922	−0.151781
0.988	−0.152410	1.059	−0.153083	1.135	−0.153804
1.217	−0.154576	1.304	−0.155404	1.398	−0.156291
1.499	−0.157240	1.606	−0.158256	1.722	−0.159343
1.845	−0.160507	1.978	−0.161752	2.120	−0.163085
2.273	−0.164512	2.436	−0.166038	2.611	−0.167671
2.799	−0.169418	3.000	−0.171287		

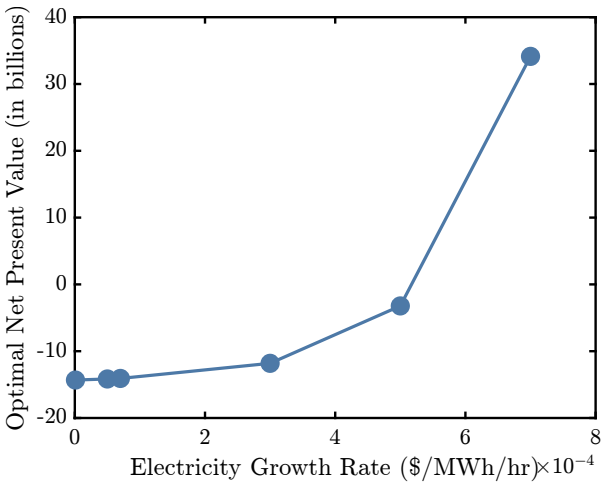

Figure 3.20: Case Study III: Sensitivity of NPV to electricity prices

Table 3.13: Case Study III: Sensitivity of NPV to electricity price multiplier

Electricity Price Multiplier	**NPV (10^9)**
Optimal	-14.95
1.000e−6	-14.32
5.000e−5	-14.16
7.000e−5	-14.08
3.000e−4	-11.82
5.000e−4	-3.22
7.000e−4	34.13

3.4.4 Sensitivity Analysis of Case Study III

The NPV of the Case Study III configuration is greatly influenced by changes in the price of electricity. Higher electricity price multipliers cause the NPV to grow nonlinearly, as Figure 3.20 shows. The system is economically unviable at the baseline value that corresponds to an NPV of -14.95×10^9 [$]. With NPV growing to -14.32×10^9 [$], a relative gain of about 4.21%, even small increases in the rate of price growth, up to 7×10^{-5}, yield clear improvement. Beyond this point, more important changes occur: increasing the multiplier to 5×10^{-4} results in a transition to positive NPV 3.22×10^9 [$], and at 7×10^{-4}, NPV leaps to 34.13×10^9 [$], improving over 328% relative to the baseline loss (see Table 3.13). This trend validates the great sensitivity of the system to assumptions about electricity prices.

The sensitivity of NPV to the storage variable O&M cost multiplier (VOM_S) reveals a threshold response with limited economic variability. NPV increases modestly to -14.90×10^9 [$] for multipliers below approximately 0.12, representing a 0.33% improvement from the baseline value of -14.95×10^9 [$], but it drops to -15.00×10^9 [$] beyond this point and remains constant. This plateau indicates that the system is tolerant to minor reductions in variable O&M costs, yet becomes insensitive to further increases, suggesting diminishing financial sensitivity to storage operating costs over a wide multiplier range.

Furthermore shown by Figures 3.21a and 3.21b is that changing the storage fixed O&M cost multiplier (C_{fom_S}) and the storage overnight capital cost multiplier (C_{occ_S}) has no appreciable effect on the economic result. The net present value stays constant at the baseline level of almost -15.3×10^9 [$] for the whole range of tested multipliers. This invariance shows that neither the optimal storage capacity nor the project-level profitability of the Case Study III configuration depends on storage-related fixed expenses or capital expenditures.

The generator overnight capital cost multiplier (C_{occ_G}) and variable O&M multiplier (C_{vom_G}) exhibit distinct influences on net present value (NPV), as seen in Table 3.16, Table 3.15, and Figure 3.22. NPV declines almost linearly and substantially with increasing C_{occ_G}, falling from 2.00×10^9 [$] at a multiplier of 0.10 to -2.00×10^9 [$] at 3.00, thus indicating a severe $200\%+$ drop that highlights strong sensitivity to capital cost assumptions. Even moderate increases (e.g., $C_{\text{occ}_G} = 1.50$) drive the NPV toward zero, emphasizing the system's financial vulnerability to generator investment escalation. In contrast, C_{vom_G} produces a stepwise NPV response with four plateaux: *Phase I* ($C_{\text{vom}_G} \leq 1.39$) sustains the baseline NPV of -14.90×10^9 [$]; *Phase II* ($1.40 \leq C_{\text{vom}_G} \leq 2.12$) lowers NPV to -15.00×10^9 [$]; *Phase III* ($2.13 \leq C_{\text{vom}_G} \leq 3.00$) results in -15.10×10^9 [$]; and *Phase IV* (beyond $C_{\text{vom}_G} > 3.00$) causes a further drop to -15.20×10^9 [$]. Although VOM increases induce losses, the range of deterioration remains modest (within 2%), implying that financial outcomes are comparatively more robust to generator O&M escalation than to capital cost inflation.

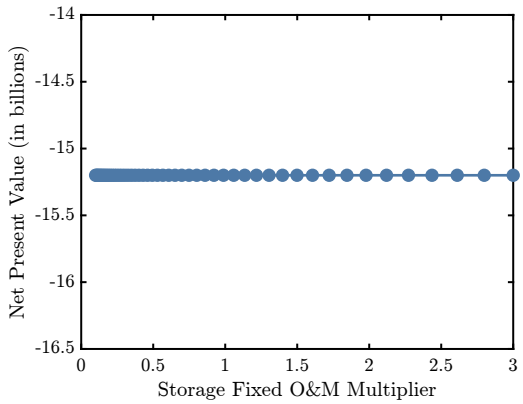

(a) Storage fixed O&M multiplier

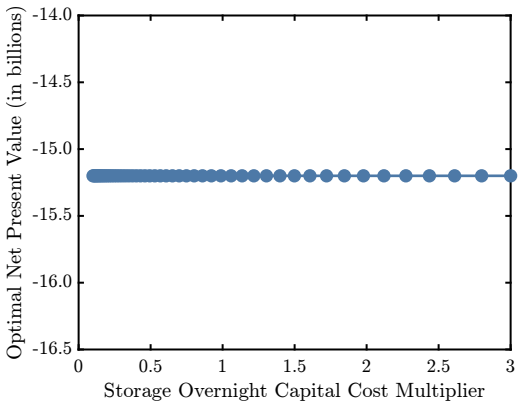

(b) Storage OCC multiplier

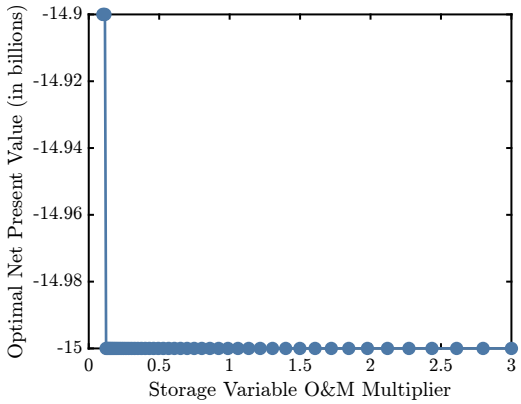

(c) Storage variable O&M multiplier

Figure 3.21: Case Study III: Sensitivity of NPV to storage cost multipliers

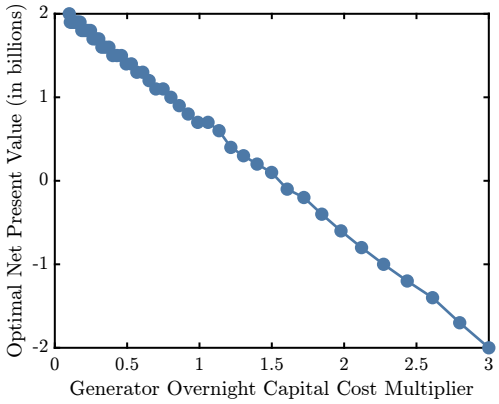

(a) Generator OCC multiplier

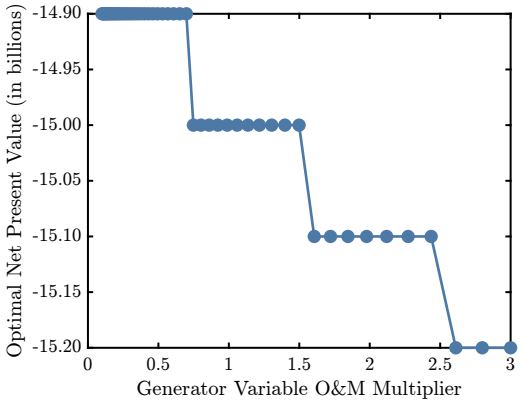

(b) Generator variable O&M multiplier

Figure 3.22: Case Study III: Sensitivity of NPV to generator cost multipliers

Table 3.14: Case Study III: Sensitivity of NPV to VOM_S scale factor

VOM_S	NPV (10^9)	VOM_S	NPV (10^9)	VOM_S	NPV (10^9)
0.100	-14.900	0.107	-14.90	0.115	-14.90
0.123	-15	0.132	-15	0.141	-15
0.152	-15	0.163	-15	0.174	-15
0.187	-15	0.200	-15	0.215	-15
0.230	-15	0.247	-15	0.264	-15
0.283	-15	0.304	-15	0.325	-15
0.349	-15	0.374	-15	0.401	-15
0.430	-15	0.460	-15	0.494	-15
0.529	-15	0.567	-15	0.608	-15
0.652	-15	0.698	-15	0.749	-15
0.802	-15	0.860	-15	0.922	-15
0.988	-15	1.059	-15	1.135	-15
1.217	-15	1.304	-15	1.398	-15
1.499	-15	1.606	-15	1.722	-15
1.845	-15	1.978	-15	2.120	-15
2.273	-15	2.436	-15	2.611	-15
2.799	-15	3.000	-15		

Table 3.15: Case Study III: Sensitivity of NPV to VOM_G scale factor

VOM_G	NPV (10^9)	VOM_G	NPV (10^9)	VOM_G	NPV (10^9)
0.100	-14.90	0.107	-14.90	0.115	-14.90
0.123	-14.90	0.132	-14.90	0.141	-14.90
0.152	-14.90	0.163	-14.90	0.174	-14.90
0.187	-14.90	0.200	-14.90	0.215	-14.90
0.230	-14.90	0.247	-14.90	0.264	-14.90
0.283	-14.90	0.304	-14.90	0.325	-14.90
0.349	-14.90	0.374	-14.90	0.401	-14.90
0.430	-14.90	0.460	-14.90	0.494	-14.90
0.529	-14.90	0.567	-14.90	0.608	-14.90
0.652	-14.90	0.698	-14.90	0.749	-14.90
0.802	-14.90	0.860	-14.90	0.922	-14.90
0.988	-14.90	1.059	-14.90	1.135	-14.90
1.217	-14.90	1.304	-14.90	1.398	-15.00
1.499	-15.00	1.606	-15.00	1.722	-15.00
1.845	-15.00	1.978	-15.00	2.120	-15.00
2.273	-15.00	2.436	-15.10	2.611	-15.10
2.799	-15.10	3.000	-15.10	3.150	-15.20
3.315	-15.20	3.486	-15.20		

Table 3.16: Case Study III: Sensitivity of NPV to C_{occ_G} multiplier

C_{occ_G} Multiplier	NPV (10^9)	C_{occ_G} Multiplier	NPV (10^9)	C_{occ_G} Multiplier	NPV (10^9)
0.100	2.00	0.107	1.90	0.115	1.90
0.123	1.90	0.132	1.90	0.141	1.90
0.152	1.90	0.163	1.90	0.174	1.90
0.187	1.80	0.200	1.80	0.215	1.80
0.230	1.80	0.247	1.80	0.264	1.70
0.283	1.70	0.304	1.70	0.325	1.60
0.349	1.60	0.374	1.60	0.401	1.50
0.430	1.50	0.460	1.50	0.494	1.40
0.529	1.40	0.567	1.30	0.608	1.30
0.652	1.20	0.698	1.10	0.749	1.10
0.802	1.00	0.860	0.90	0.922	0.80
0.988	0.70	1.059	0.70	1.135	0.60
1.217	0.40	1.304	0.30	1.398	0.20
1.499	0.10	1.606	−0.10	1.722	−0.20
1.845	−0.40	1.978	−0.60	2.120	−0.80
2.273	−1.00	2.436	−1.20	2.611	−1.40
2.799	−1.70	3.000	−2.00		

Table 3.17: Case Study III: Sensitivity of storage capacity to OCC_S multiplier

OCC_S Multiplier	Storage (MWh)	OCC_S Multiplier	Storage (MWh)	OCC_S Multiplier	Storage (MWh)
0.100	1248735.7	0.107	1164050.0	0.115	1080239.1
0.123	1033005.9	0.132	951660.0	0.141	894964.3
0.152	839700.0	0.163	791115.1	0.174	746824.1
0.187	697603.0	0.200	643054.3	0.215	594708.0
0.230	559800.0	0.247	530617.2	0.264	497379.1
0.283	454519.4	0.304	442591.9	0.325	415317.5
0.349	387089.0	0.374	362438.7	0.401	334448.7
0.430	307890.0	0.460	283239.7	0.494	279900.0
0.529	254295.5	0.567	254057.0	0.608	227498.3
0.652	225828.4	0.698	223920.0	0.749	223920.0
0.802	197838.4	0.860	197599.9	0.922	195930.0
0.988	195930.0	1.059	195930.0	1.135	169371.3
1.217	169371.3	1.304	169371.3	1.398	167940.0
1.499	167940.0	1.606	141142.8	1.722	141142.8
1.845	139950.0	1.978	139950.0	2.120	112914.2
2.273	112914.2	2.436	111960.0	2.611	111960.0
2.799	111960.0	3.000	84685.7		

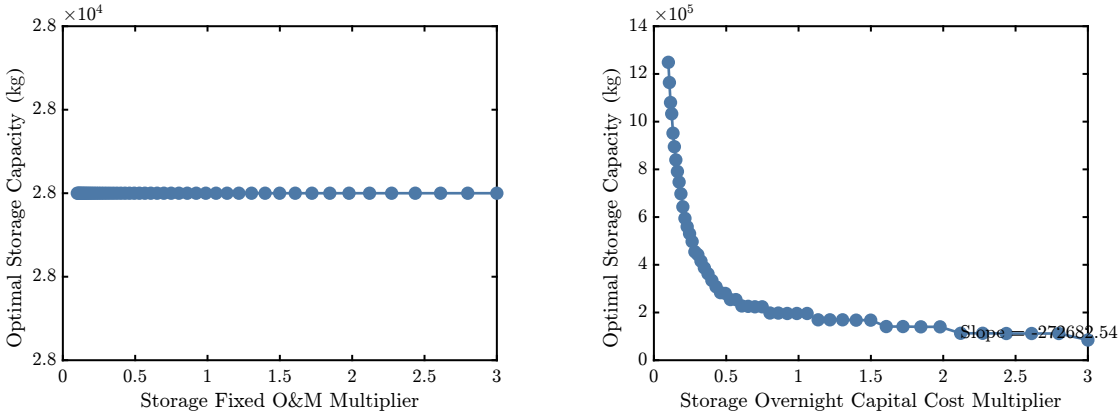

(a) Storage fixed O&M multiplier

(b) Storage overnight capital cost multiplier

Figure 3.23: Case Study III: Sensitivity of optimal storage capacity to cost multipliers

Figure 3.23 and Table 3.17 illustrate the sensitivity of optimal storage capacity to variations in two cost multipliers: the storage fixed O&M cost multiplier (C_{fom_S}) and the storage overnight capital cost multiplier (C_{occ_S}).

As shown in Figure 3.23a, changes in C_{fom_S} have virtually no effect on the optimal storage capacity, which remains constant at approximately $28{,}000$ [kg] across the entire multiplier range. This indicates that the system is largely insensitive to variations in fixed storage O&M costs.

By contrast, Figure 3.23b shows a strong inverse relationship between C_{occ_S} and the optimal storage capacity. At low values of the multiplier (e.g., 0.1), the optimal capacity reaches as high as 1.25×10^6 [kg]. As the multiplier increases, capacity declines rapidly, approaching a lower bound of around $84{,}686$ [kg] at $C_{\text{occ}_S} = 3.0$. The curve exhibits a steep nonlinear drop in the lower range of the multiplier, followed by a gradual flattening, indicating diminishing sensitivity at higher cost levels. These findings highlight that storage investment decisions are highly sensitive to capital cost assumptions, but not to fixed O&M expenses.

3.4.5 Summary and Comparison of Sensitivity Studies

Tables 3.18, 3.19, and 3.20 synthesize the results of the sensitivity analyses across the three case studies; visually compiled in Figures 3.24, 3.25, and 3.26. These together show how changes in important input factors influence the optimal NPV under several system and policy settings.

Summary for Case Study I

According to the sensitivity results of Case Study I, NPV is most susceptible to fluctuations in *electricity prices* and *generator capital cost*. Table 3.18 shows that a considerable positive change in NPV results from increases in the electricity price multiplier, reaching up to **+321%** in the capped case, which excludes extreme outliers for visual clarity. On the other hand, generator capital cost ($C_{\text{occ},G}$) exhibits the strongest bidirectional influence, with NPV varying from **+89.2%** to **–198.2%** depending on the input range. Although carbon tax increases reduce NPV, their overall impact remains modest (around **–4.4%**), while the effects of natural gas price and generator variable O&M cost ($C_{\text{vom},G}$) remain limited to under **–1.5%** and **–1.0%**, respectively. Storage-related costs — including fixed O&M, CapEx, and variable O&M — have virtually no measurable effect. The tornado plot in Figure 3.24 visually confirms these trends.

Summary for Case Study II

The sensitivity results of Case Study II emphasize considerably *lower overall sensitivity* compared to Case Study I. Storage-related cost variations — including fixed O&M ($C_{\text{fom},S}$), capital cost ($C_{\text{occ},S}$), and variable O&M ($C_{\text{vom},S}$) — show *insignificant to very minor* influence on NPV, with changes remaining within a narrow band of $\pm 1\%$ (see Table 3.19). Generator capital cost ($C_{\text{occ},G}$) causes a slightly more noticeable decline of around -2.8%, yet still reflects strong system robustness. The most significant impact is observed for generator variable O&M cost ($C_{\text{vom},G}$), which reduces NPV by up to 16%, indicating a moderate but consistent sensitivity. These outcomes align well with the tornado plot shown in Figure 3.25, confirming the stable economic behavior of the system under a wide range of cost fluctuations.

Summary for Case Study III

The sensitivity results of Case Study III underscore the dominant role of electricity price assumptions in determining the net present value (NPV) of the system. As summarized in Table 3.20, electricity price variations cause substantial swings in economic performance, with gains reaching

up to **+321%**. This is visually evident in Figure 3.26, where the electricity price bar sharply outweighs all others.

The generator capital cost multiplier ($C_{\mathrm{occ},G}$) follows closely behind in terms of impact. Increases in generator CapEx lead to dramatic reductions in NPV, with a maximum observed drop of **–229%**. This reflects the system's financial vulnerability to capital investment escalations in generation infrastructure.

By contrast, changes in storage-related cost multipliers — including fixed O&M ($C_{\mathrm{fom},S}$), capital expenditures ($C_{\mathrm{occ},S}$), and variable O&M ($C_{\mathrm{vom},S}$) — have little to no effect on NPV, confirming the system's insensitivity to storage cost variations in this configuration. These inputs cause NPV shifts within a narrow range of **±0.7%** or less, underscoring their limited economic leverage.

Generator variable O&M costs ($C_{\mathrm{vom},G}$) produce small and nonlinear changes in NPV (maximum of **+1.3%** gain and **–0.7%** loss), implying that while operational expenses in generation affect profitability, their influence remains secondary compared to CapEx and electricity pricing.

Overall, Case Study III reinforces the central conclusion from earlier cases: the economic feasibility of such energy systems depends heavily on generator investment levels and electricity market assumptions, with storage-related cost parameters playing a minimal role under the modeled assumptions.

Table 3.18: Case Study I: Sensitivity of NPV to parameter changes

Parameter	Input Change Range (%)	Output Change Range (% NPV)
Carbon Tax	0% to $+438\%$	$+3.0\%$ to -4.4%
Natural Gas Price	$+0.01\%$ to $+90\%$	-0.9% to -1.5%
Electricity Price	$+0.0001\%$ to $+70{,}000\%$	$+0.6\%$ to $+321\%$
$C_{\text{occ},G}$	-90% to $+200\%$	$+89.2\%$ to -198.2%
$C_{\text{vom},G}$	-90% to $+200\%$	0.0% to -1.0%

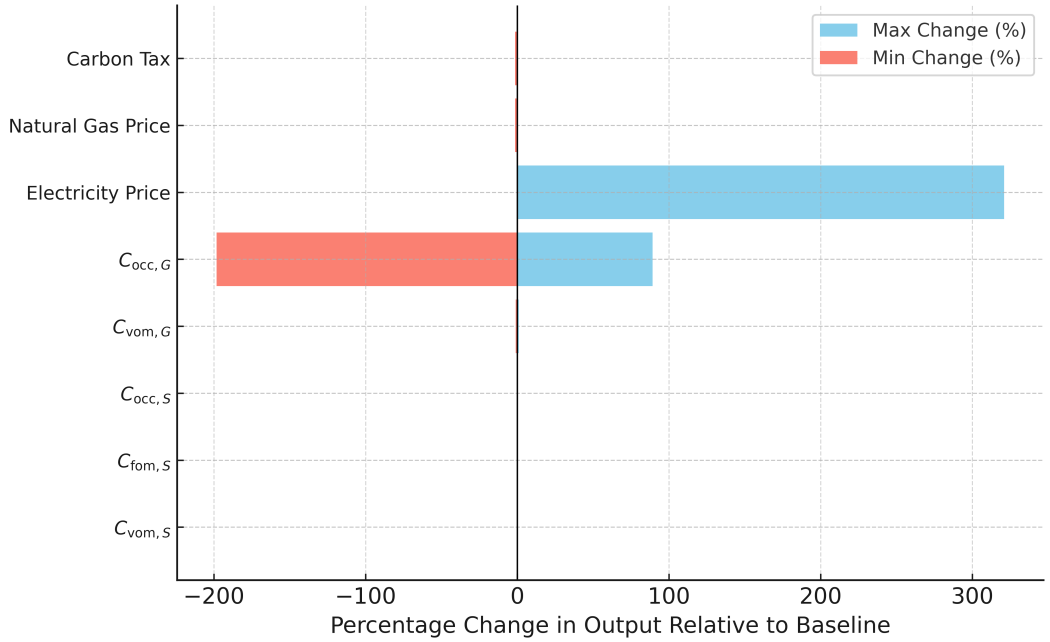

Figure 3.24: Case Study I: Sensitivity plot of optimal NPV to select optimization model inputs

Table 3.19: Case Study II: Sensitivity of NPV to parameter changes

Parameter	Input Change Range (%)	NPV Change Range (%)
$C_{\text{vom},G}$	0% to $+300\%$	-16.0%
$C_{\text{occ},S}$	0% to $+300\%$	-0.77% to -0.86%
$C_{\text{vom},S}$	0% to $+300\%$	-0.16% to -0.17%
$C_{\text{occ},G}$	0% to $+300\%$	-2.83%
$C_{\text{fom},S}$	0% to $+300\%$	0.0%

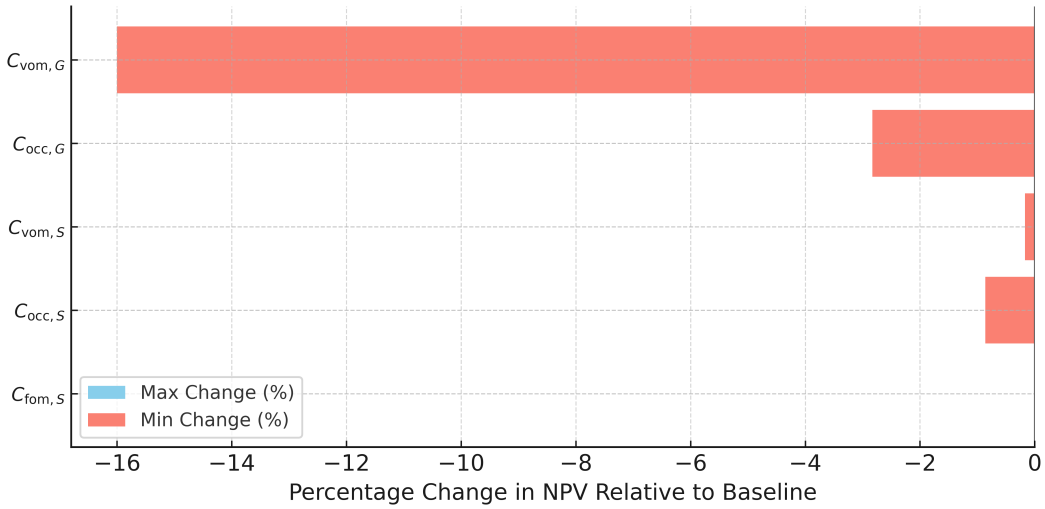

Figure 3.25: Case Study II: Sensitivity plot of optimal NPV to select optimization model inputs

Table 3.20: Case Study III: Sensitivity of NPV to parameter changes

Parameter	Input Change Range (%)	NPV Change Range (%)
Electricity Price	-99% to $+400\%$	$+7\%$ to $+321\%$
$C_{\text{occ},G}$	-90% to $+200\%$	-229%
$C_{\text{vom},G}$	-90% to $+200\%$	$+1.3\%$ to -0.7%
$C_{\text{occ},S}$	-90% to $+200\%$	0%
$C_{\text{fom},S}$	-90% to $+200\%$	0%
$C_{\text{vom},S}$	-90% to $+200\%$	$+0.7\%$ to -0.7%

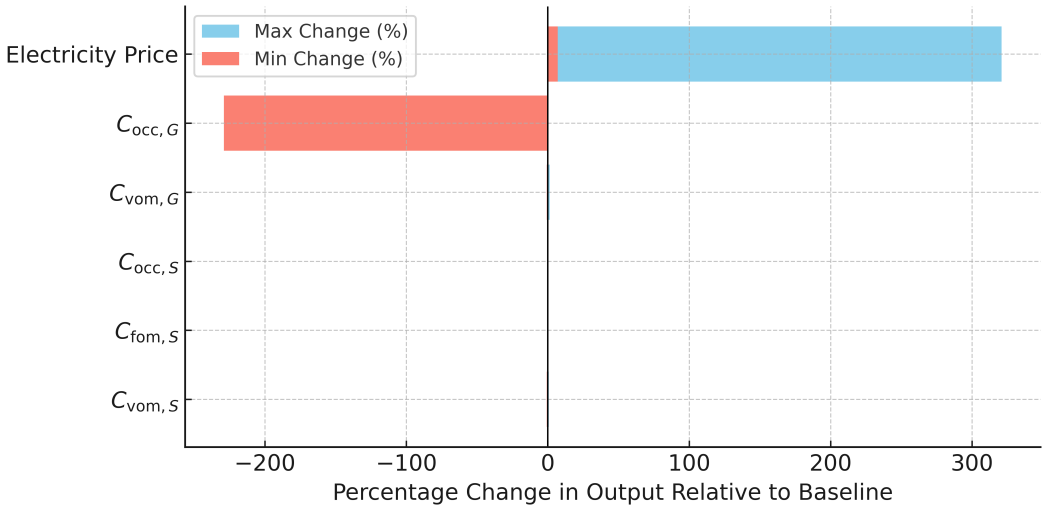

Figure 3.26: Case Study III: Sensitivity plot of optimal NPV to select optimization model inputs

Chapter 4

Conclusion

4.1 Summary

This work provides a suitable methodology to evaluate the combined generator and storage energy system economic viability. Under the suggested paradigm, ECOGEN-CCD, early-stage evaluation of several Integrated Energy System (IES) configurations is possible. Under stated technical and financial assumptions, the framework finds ideal technology parameters and operational strategies by using a system-level, control co-design method. Designed to assist both new projects and retrofit initiatives, ECOGEN-CCD helps engineers, financiers, and stakeholders make decisions and communicate with one another.

Three case examples are used to highlight ECOGEN-CCD's potential. Examining a natural gas combined cycle (NGCC) power station coupled with thermal energy storage (TES) and a carbon capture system (CCS), Case Study I looked at operational complexity connected to non-dispatchable renewable resources. Case Study II concentrated on a wind farm combined with a battery energy storage system (BESS). Case Study III evaluated a nuclear power plant (NPP) coupled with a hydrogen generating and storing system, thereby enabling flexible involvement in both the hydrogen and electricity markets.

Using hourly resolution, each case study was modeled over a 30-year operating horizon; the optimization problem was developed as a linear, convex problem, hence facilitating effective identification of the global optimal solution. The strength of the framework was assessed using a sensitivity analysis. The effects of changes in market pricing, capital and operational expenses, and demand-following limitations on the ideal system configurations and financial results were investigated in this paper. The sensitivity analysis results verified that external market and policy circumstances clearly affect storage size and economic performance. By means of a thorough and scalable instrument for assessing the long-term viability of integrated energy systems, ECOGEN-

CCD offers by means of complete techno-economic modeling and sensitivity analysis integration. Its flexibility and efficiency make it suitable for application in strategic energy planning and investment analysis under uncertainty.

4.2 Future Work

Future research should seek to enlarge the present framework in numerous important dimensions to improve realism, applicability, and decision-support capacity. First, the model could be extended to support the co-sizing and co-dispatch of mixed-portfolio hybrid energy systems. This includes multiple generation sources such as nuclear, natural gas, wind, and solar, and it also incorporates a suite of complementary storage technologies, including lithium-ion batteries, thermal energy storage, and long-duration systems like hydrogen or compressed air. This would allow a more realistic depiction of actual hybrid plants and expose value synergies between technologies that the current formulation cannot capture. Further improving operational realism would include adding higher-fidelity physics, starting costs, cycle deterioration, and ramp rate limits, along with finer temporal resolution (e.g., 5- to 15-minute intervals). Under real-world variability, including stochastic or resilient optimization approaches to manage uncertainty in renewables and price signals might help to further increase the dependability of the suggested solutions. Beyond modeling, by including real-time data on deterioration, response dynamics, and practical limits, validation via hardware-in-the-loop experiments at pilot-scale facilities might hone control algorithms. By including the optimization engine within a larger model-based systems engineering (MBSE) framework, one might simultaneously address stakeholder, regulatory, and techno-economic needs, hence enabling thorough examination of system trade-offs. These guidelines, taken together, point toward a verified, multi-objective platform able to steer the design and implementation of hybrid energy systems of future generations.

Bibliography

[1] J. Wu, J. Yan, H. Jia *et al.*, "Integrated energy systems," *Applied Energy*, vol. 167, pp. 155–157, Apr. 2016, doi: 10.1016/j.apenergy.2016.02.075.

[2] A. E. H. Berjawi, S. L. Walker, C. Patsios, and S. H. R. Hosseini, "An evaluation framework for future integrated energy systems: A whole energy systems approach," *Renewable and Sustainable Energy Reviews*, vol. 145, p. 111163, Jul. 2021, doi: 10.1016/j.rser.2021.111163.

[3] S. Pfenninger, A. Hawkes, and J. Keirstead, "Energy systems modeling for twenty-first century energy challenges," *Renewable and Sustainable Energy Reviews*, vol. 33, pp. 74–86, May 2014, doi: 10.1016/j.rser.2014.02.003.

[4] T. Zhang, "Techno-economic analysis of a nuclear-wind hybrid system with hydrogen storage," *Journal of Energy Storage*, vol. 46, p. 103807, Feb. 2022, doi: 10.1016/j.est.2021.103807.

[5] J. Wang, J. Mao, R. Hao, S. Li, and G. Bao, "Multi-energy coupling analysis and optimal scheduling of regional integrated energy system," *Energy*, vol. 254, p. 124482, Sep. 2022, doi: 10.1016/j.energy.2022.124482.

[6] J. Xiao, Z. Li, C. Song, and C. Wang, "Energy coupling of integrated energy system:indicators, observation method and mechanism," *SSRN Electronic Journal*, 2024, preprint. doi: 10.2139/ssrn.4748206.

[7] X. Wang and F. Blaabjerg, "Harmonic stability in power electronic-based power systems: Concept, modeling, and analysis," *IEEE Transactions on Smart Grid*, vol. 10, no. 3, pp. 2858–2870, May 2019, doi: 10.1109/TSG.2018.2812712.

[8] P. Taylor, M. Abeysekera, Y. Bian *et al.*, "An interdisciplinary research perspective on the future of multi-vector energy networks," *International Journal of Electrical Power & Energy Systems*, vol. 135, p. 107492, Feb. 2022, doi: 10.1016/j.ijepes.2021.107492.

[9] P. Colbertaldo, F. Parolin, and S. Campanari, "A comprehensive multi-node multi-vector multi-sector modelling framework to investigate integrated energy systems and assess decarbonisation needs," *Energy Conversion and Management*, vol. 291, p. 117168, Sep. 2023, doi: 10.1016/j.enconman.2023.117168.

[10] I. Sorrenti, T. B. Harild Rasmussen, S. You, and Q. Wu, "The role of power-to-x in hybrid renewable energy systems: A comprehensive review," *Renewable and Sustainable Energy Reviews*, vol. 165, p. 112380, Sep. 2022, doi: 10.1016/j.rser.2022.112380.

[11] G. Li and X. Zheng, "Thermal energy storage system integration forms for a sustainable future," *Renewable and Sustainable Energy Reviews*, vol. 62, pp. 736–757, Sep. 2016, doi: 10.1016/j.rser.2016.04.076.

[12] E. J. Markey, R. Vercellino, B. J. Limb *et al.*, "Economic impact of thermal energy storage on natural gas power with carbon capture in future electricity markets," *International Journal of Greenhouse Gas Control*, vol. 133, p. 104098, Mar. 2024, doi: 10.1016/j.ijggc.2024.104098.

[13] J. Wang, H. Zhong, Z. Ma, Q. Xia, and C. Kang, "Review and prospect of integrated demand response in the multi-energy system," *Applied Energy*, vol. 202, pp. 772–782, Sep. 2017, doi: 10.1016/j.apenergy.2017.05.150.

[14] T. M. Alabi, E. I. Aghimien, F. D. Agbajor *et al.*, "A review on the integrated optimization techniques and machine learning approaches for modeling, prediction, and decision making on integrated energy systems," *Renewable Energy*, vol. 194, pp. 822–849, Jul. 2022, doi: 10.1016/j.renene.2022.05.123.

[15] J. A. Huyett, Z. G. Gulumjanli, R. G. Koldyke *et al.*, "Engineering and design of an integrated thermal storage and carbon capture system on Calpine's Delta Energy Center," in *Greenhouse Gas Control Technologies Conference*, Oct. 2024, doi: 10.2139/ssrn.5035090.

[16] C. Qin, Q. Yan, and G. He, "Integrated energy systems planning with electricity, heat and gas using particle swarm optimization," *Energy*, vol. 188, p. 116044, Dec. 2019, doi: 10.1016/j.energy.2019.116044.

[17] X. Zhao, W. Zheng, Z. Hou *et al.*, "Economic dispatch of multi-energy system considering seasonal variation based on hybrid operation strategy," *Energy*, vol. 238, p. 121733, Jan. 2022, doi: 10.1016/j.energy.2021.121733.

[18] P. Horrillo-Quintero, P. García-Triviño, C. E. Ugalde-Loo *et al.*, "Efficient energy dispatch in multi-energy microgrids with a hybrid control approach for energy management system," *Energy*, vol. 317, p. 134599, Feb. 2025, doi: 10.1016/j.energy.2025.134599.

[19] S. Lu, W. Gu, J. Zhou, X. Zhang, and C. Wu, "Coordinated dispatch of multi-energy system with district heating network: Modeling and solution strategy," *Energy*, vol. 152, pp. 358–370, Jun. 2018, doi: 10.1016/j.energy.2018.03.088.

[20] H. Tang and S. Wang, "A model-based predictive dispatch strategy for unlocking and optimizing the building energy flexibilities of multiple resources in electricity markets of multiple services," *Applied Energy*, vol. 305, p. 117889, Jan. 2022, doi: 10.1016/j.apenergy.2021.117889.

[21] R. Evins, K. Orehounig, V. Dorer, and J. Carmeliet, "New formulations of the 'energy hub' model to address operational constraints," *Energy*, vol. 73, pp. 387–398, Aug. 2014, doi: 10.1016/j.energy.2014.06.029.

[22] D. J. Arent, S. M. Bragg-Sitton, D. C. Miller *et al.*, "Multi-input, multi-output hybrid energy systems," *Joule*, vol. 5, no. 1, pp. 47–58, Jan. 2021, doi: 10.1016/j.joule.2020.11.004.

[23] D. McDowell, P. Talbot, A. Wrobel *et al.*, "A technical and economic assessment of LWR flexible operation for generation and demand balancing to optimize plant revenue," Idaho National Laboratory, Tech. Rep. INL/EXT-21-65443-Revision-1, Dec. 2021, doi: 10.2172/1844211.

[24] I. Khamis and U. D. Malshe, "HEEP: A new tool for the economic evaluation of hydrogen economy," *International Journal of Hydrogen Energy*, vol. 35, no. 16, pp. 8398–8406, Aug. 2010, doi: 10.1016/j.ijhydene.2010.04.154.

[25] M. Garcia-Sanz, "Control co-design: An engineering game changer," *Advanced Control for Applications*, vol. 1, no. 1, p. e18, Oct. 2019, doi: 10.1002/adc2.18.

[26] R. Vercellino, E. Markey, B. J. Limb *et al.*, "Control co-design optimization of natural gas power plants with carbon capture and thermal storage," in *ASME International Design Engineering Technical Conferences*, no. DETC2022-90021, Aug. 2022, doi: 10.1115/detc2022-90021.

[27] G. J. Soto Gonzalez and P. W. Talbot, "FORCE-DISPATCHES integration - initial demonstration," Idaho National Laboratory, Tech. Rep. INL/RPT-22-69033-Rev000, Sep. 2022, doi: 10.2172/1891636.

[28] B. Li, P. W. Talbot, D. McDowell, and J. K. Hansen, "Release a public version of HERON (HERON 2.0) with improved algorithms for the treatment of energy storage," Idaho National Laboratory, Tech. Rep. INL/EXT-21-65473-Rev000, Dec. 2021, doi: 10.2172/1838610.

[29] S. Lu, Y. Li, W. Gu, Y. Xu, and S. Ding, "Economy-carbon coordination in integrated energy systems: Optimal dispatch and sensitivity analysis," *Applied Energy*, vol. 351, p. 121871, Dec. 2023, doi: 10.1016/j.apenergy.2023.121871.

[30] A. Ashouri, F. Petrini, R. Bornatico, and M. J. Benz, "Sensitivity analysis for robust design of building energy systems," *Energy*, vol. 76, pp. 264–275, Nov. 2014, doi: 10.1016/j.energy.2014.07.095.

[31] J. Dancker, C. Klabunde, and M. Wolter, "Sensitivity factors in electricity-heating integrated energy systems," *Energy*, vol. 229, p. 120600, Aug. 2021, doi: 10.1016/j.energy.2021.120600.

[32] D. R. Herber, "Advances in combined architecture, plant, and control design," Ph.D. Dissertation, University of Illinois at Urbana-Champaign, Urbana, IL, USA, Dec. 2017, url: http://hdl.handle.net/2142/99394.

[33] "DT QP project," GitHub, url: https://github.com/danielrherber/dt-qp-project.

[34] "ECOGEN-CCD," GitHub, url: https://github.com/AzadSaeed/ECOGEN-CCD/releases/tag/v1.0.0.

[35] P. L. Joskow and J. E. Parsons, "The economic future of nuclear power," *Daedalus*, vol. 138, no. 4, pp. 45–59, Sep. 2009, doi: 10.1162/daed.2009.138.4.45.

[36] H. Mantripragada and E. S. Rubin, "Techno-economic analysis methods for nuclear power plants," USAEE, Working Paper 18-346, Jun. 2018, doi: 10.2139/ssrn.3198421.

[37] IAEA, "Approaches for assessing the economic competitiveness of small and medium sized reactors," International Atomic Energy Agency, IAEA Nuclear Energy Series No. NP-T-3.7, 2013.

[38] B. Wealer, S. Bauer, C. Hirschhausen, C. Kemfert, and L. Göke, "Investing into third generation nuclear power plants - review of recent trends and analysis of future investments using monte carlo simulations," *Renewable and Sustainable Energy Reviews*, vol. 143, p. 110836, Jun. 2021, doi: 10.1016/j.rser.2021.110836.

[39] J. R. R. A. Martins and A. Ning, *Engineering Design Optimization*. Cambridge University Press, Nov. 2021, doi: 10.1017/9781108980647.

[40] D. R. Herber and J. T. Allison, "Unified scaling of dynamic optimization design formulations," in *ASME International Design Engineering Technical Conferences*, no. DETC2017-67676, Aug. 2017, doi: 10.1115/detc2017-67676.

[41] E. S. Rubin and H. Zhai, "The cost of carbon capture and storage for natural gas combined cycle power plants," *Environmental Science & Technology*, vol. 46, no. 6, pp. 3076–3084, Mar. 2012, doi: 10.1021/es204514f.

[42] B. J. Limb, E. Markey, R. Vercellino *et al.*, "Economic viability of using thermal energy storage for flexible carbon capture on natural gas power plants," *Journal of Energy Storage*, vol. 55, p. 105836, Nov. 2022, doi: 10.1016/j.est.2022.105836.

[43] U.S. Energy Information Administration, "Capital cost and performance characteristic estimates for utility scale electric power generating technologies," U.S. Department of Energy, Report SL-014940, Feb. 2020.

[44] "gridstatus," Online, url: https://opensource.gridstatus.io.

[45] U.S. Energy Information Administration, "Henry hub natural gas spot price data," Online, url: https://www.eia.gov/dnav/ng/hist/rngwhhdm.htm.

[46] J. D. Jenkins, S. Chakrabarti, F. Cheng, and P. Neha, "Summary report of the GenX and PowerGenome runs for generating price series (for ARPA-E FLECCS project)," Zenodo, Version v1, Dec. 2021, doi: 10.5281/ZENODO.5765798.

[47] "GenX," GitHub, url: https://github.com/GenXProject/GenX.

[48] M. Jannati and B. Vahidi, "A master-slave adaptive linear neuron-based approach for cost-effective use of battery energy storage systems in wind farms," *Results in Engineering*, vol. 23, p. 102410, Sep. 2024, doi: 10.1016/j.rineng.2024.102410.

[49] Q. Jiang, Y. Gong, and H. Wang, "A battery energy storage system dual-layer control strategy for mitigating wind farm fluctuations," *IEEE Transactions on Power Systems*, vol. 28, no. 3, pp. 3263–3273, Aug. 2013, doi: 10.1109/TPWRS.2013.2244925.

[50] British Petroleum, "BP statistical review of world energy," BP, Tech. Rep., Jun. 2016.

[51] International Energy Agency, "The future of hydrogen," IEA, Tech. Rep., Jun. 2019, url: https://www.iea.org/reports/the-future-of-hydrogen.

[52] S. Hancock and T. Westover, "Simulation of 15% and 50% thermal power dispatch to an industrial facility using a flexible generic full-scope pressurized water reactor plant simulator," *Energies*, vol. 15, no. 3, p. 1151, Feb. 2022, doi: 10.3390/en15031151.

[53] K. Frick, P. Talbot, D. Wendt *et al.*, "Evaluation of hydrogen production feasibility for a light water reactor in the Midwest," Idaho National Laboratory, Tech. Rep. INL/EXT-19-55395-Rev000, Sep. 2019, doi: 10.2172/1569271.

[54] L. Mingyi, Y. Bo, X. Jingming, and C. Jing, "Thermodynamic analysis of the efficiency of high-temperature steam electrolysis system for hydrogen production," *Journal of Power Sources*, vol. 177, no. 2, pp. 493–499, Mar. 2008, doi: 10.1016/j.jpowsour.2007.11.019.

[55] M. M. Ramadan, Y. Wang, and P. Tooteja, "Analysis of hydrogen production costs across the United States and over the next 30 years," arXiv, Jun. 2022, doi: 10.48550/ARXIV.2206.10689.

[56] D. Kryzia and L. Gawlik, "Forecasting the price of uranium based on the costs of uranium deposits exploitation," *Mineral Resources Management*, vol. 32, no. 3, pp. 93–110, Sep. 2016, doi: 10.1515/gospo-2016-0026.

[57] F. A. Settle, "Uranium to electricity: The chemistry of the nuclear fuel cycle," *Journal of Chemical Education*, vol. 86, no. 3, p. 316, Mar. 2009, doi: 10.1021/ed086p316.

[58] NEA, "Technical and economic aspects of load following with nuclear power plants," OECD, Tech. Rep., Jun. 2011, doi: 10.1787/29e7df00-en.

[59] G. MacKerron, "Nuclear costs: Why do they keep rising?" *Energy Policy*, vol. 20, no. 7, pp. 641–652, Jul. 1992, doi: 10.1016/0301-4215(92)90006-N.

Appendix A

Abbreviations and Notation

A.1 Acronyms

Table A.1: Key acronyms used in this work

Term	Description
BESS	Battery energy storage system
CCD	Control co-design
CCS	Carbon capture and storage
CHP	Combined heat and power
CO_2	Carbon dioxide
DTQP	Direct transcription (DT) and quadratic programming (QP) [33]
ECOGEN-CCD	Computational framework for economic feasibility of generator and storage systems through CCD [34]
FEL	Following electric load
FOC	Following operation cost
HES	Hybrid energy systems
HFC	Hydrogen fuel cell
HRES	Hybrid renewable energy systems
HTSE	High-temperature steam electrolysis
HVAC	Heating, ventilation, and air conditioning
IDC	Interest during construction
IES	Integrated energy systems
MEMG	Multi-energy microgrid
ML	Machine learning
MW	Megawatt
NGCC	Natural gas combined cycle
NPP	Nuclear power plant
NPV	Net present value
OC	Operational cost
OCC	Overnight capital cost
O&M	Operations and maintenance

Continued on next page

Table A.1 (continued)

Term	Description
P2G	Power-to-gas
P2X	Power-to-X
PCC	Post-combustion carbon capture
TES	Thermal energy storage

A.2 Variables

Table A.2: Key variables used in this work

Symbol	Description
C_{cap}	Capital cost
CO_2	CO_2 penalty (price)
C_E	Electricity price signal
C_{fom}	Fixed O&M cost
C_{fuel}	Fuel price signal
C_P	Primary price signal
C_T	Tertiary price signal
C_{vom}	Variable O&M cost
E_{fuel}	Fuel expenditure
L	Load
n	Node index
R	Revenue
r	Discount rate
T_{con}	Construction time
$\boldsymbol{u}$	Control vector
$\overrightarrow{u}$	Charging signal
$\overleftarrow{u}$	Discharging signal
$\boldsymbol{x}$	State vector
$\boldsymbol{\Sigma}$	Storage capacity
$\overrightarrow{\eta}$	Charge efficiency
$\overleftarrow{\eta}$	Discharge efficiency

A.3 Subscripts / Indices

Table A.3: Key subscripts / indices used in this work

Symbol	Description
$\bullet_E$	Index for electrical domain
$\bullet_G$	Index for generator
$\bullet_P$	Index for primary domain
$\bullet_R$	Index for revenue
$\bullet_S$	Index for storage
$\bullet_T$	Index for tertiary domain